Rigid foldability is NP-hard

RIGID FOLDABILITY IS NP-HARD

Hugo A. Akitaya,[*] *Erik D. Demaine,*[†] *Takashi Horiyama,*[‡] *Thomas C. Hull,*[§] *Jason S. Ku,*[¶] *and Tomohiro Tachi*[‖]

ABSTRACT. We prove NP-hardness of deciding rigid foldability, that is, whether a sheet of material can be folded by bending only at prescribed creases while all regions between the creases undergo a rigid motion, like rigid plates connected at hinges. First, given a degree-4 flat-foldable crease pattern, deciding whether exactly those creases can be flexed (with every specified crease bending nontrivially), up to a given ε accuracy, is weakly NP-complete by a reduction from Partition. Second, given a crease pattern, deciding whether there is a rigid folding bending at any nonempty subset of those creases (i.e., where each crease is optional) is strongly NP-hard by a reduction from Positive 1-in-E3 SAT. Both results hold when just looking for a small motion adjacent to the unfolded 2D state, where there is no potential for self-intersection of the material. Thus our results are quite unlike existing NP-hardness results for flat foldability of crease patterns, where the complexity originates from finding a layer ordering that avoids self-intersection. Rather, our hardness proofs exploit the multiple combinatorial behaviors of rigid foldings locally at each vertex. These results justify why rigid origami has been so difficult to analyze mathematically, and help explain why it is often harder to fold from an unfolded sheet than to unfold a folded state back to 2D, a problem frequently encountered when realizing folding-based systems such as self-folding matter and reconfigurable robots.

KEYWORDS. rigid origami, computational complexity, crease pattern

1 Introduction

Informally, *rigid origami* consists of rigid polygonal panels connected at rotational edge hinges; refer to Figure 1. Given such an assembly, a *rigid folding motion* is a continuous deformation that just translates or rotates each panel (thus not deforming each panel, folding only at the hinges) and that maintains connectivity at the hinges (thus not pulling apart two hinged-together panels). *Rigid foldability* is the problem of deciding whether a given

[*]Department of Computer Science, Carleton University, Ottawa, Canada, hugoakitaya@gmail.com

[†]Computer Science and Artificial Intelligence Laboratory, Massachusetts Institute of Technology, 32 Vassar St., Cambridge, MA 02139, USA, edemaine@mit.edu

[‡]Faculty of Information Science and Technology, Hokkaido University, N14W9, Kita-ku, Sapporo, Hokkaido, 060-0814, Japan, horiyama@ist.hokudai.ac.jp

[§]Department of Mathematics, Western New England University, 1215 Wilbraham Road, Springfield, MA 01119, USA, thull@wne.edu

[¶]Department of Electrical Engineering and Computer Science, Massachusetts Institute of Technology, 77 Massachusetts Ave., Cambridge, MA 02139, USA, jasonku@mit.edu

[‖]Department of General Systems Studies, The University of Tokyo, 3-8-1 Komaba, Meguro-ku, Tokyo 153-8902, Japan, tachi@idea.c.u-tokyo.ac.jp

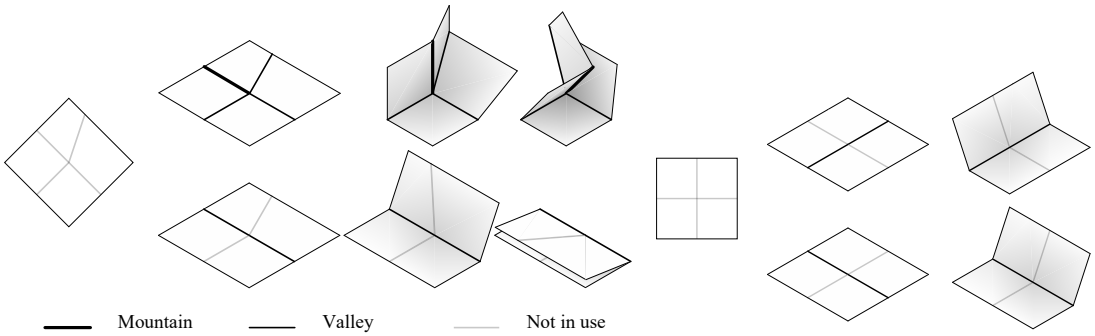

Figure 1: Left: a single vertex origami that is rigidly foldable using all creases. The pattern can be folded using all creases (top) as well as using a subset of creases (bottom). Right: a single vertex origami that is rigidly foldable with optional creases, but not using all creases.

rigid origami has any such motion, other than a trivial global translation or rotation (which does not rotate any of the hinges).

Practically, rigid origami is a mechanism whose flexibility does not rely on irreversible deformation of materials; it relies only on rotations around predefined hinges. It therefore has broad applications in different fields with various materials at different scales, for example, self-folding mechanisms of microscopic material [27], foldable packaging [9], transformable adaptive architecture with thick panels [29], and deployable space structures [26].

Despite its usefulness, we have few general mathematical results about rigid foldability. We have an efficient characterization of rigid foldability for *single-vertex* crease patterns (where all creases/hinges emanate from a common vertex) [1], and positive results for certain families of crease patterns [28]. But there is no efficient characterization or hardness result for characterizing rigid foldability of arbitrary crease patterns. This status is in contrast to *flat foldability* (deciding whether a given crease pattern can be instantaneously folded into a flat state that bends all creases by $\pm 180°$, ignoring folding motions), which has been well-studied since the first paper on computational origami [5]: we have an efficient characterization of flat foldability for single-vertex crease patterns [19, 11], and NP-hardness for general crease patterns [5, 3] even when the crease pattern is a subset of a square grid with diagonals [3].

Our objective is to determine the computational complexity of rigid foldability for a general crease pattern on a planar sheet of material (defined by a planar graph drawn with noncrossing straight-line edges on a polygon of material). Specifically, we distinguish and analyze two types of rigid foldability:

Rigid foldability with optional creases: As described informally above, a *rigid folding motion* of a crease pattern is a continuous transformation of the sheet of material (i.e., a continuous mapping from points on the material and times in $[0, 1]$ to points in $\mathbb{R}^3$) that is extrinsically isometric (a rigid-body motion of $\mathbb{R}^3$) when restricted to each face of the crease pattern (region outlined by creases and/or material boundary). A crease pattern is *rigidly foldable with optional creases* if it has a rigid folding motion that is not a global rigid-body motion of $\mathbb{R}^3$.

Which creases?	Crease pattern family	Precision	Lower bound	Upper bound
Optional creases	General	Exact	Strongly NP-hard	$\exists\mathbb{R}$
Optional creases	Degree-4 flat-foldable	Exact		NP
Optional creases	Degree-4 flat-foldable	Finite precision	Weakly NP-hard	NP
All creases	General	Exact		$\exists\mathbb{R}$
All creases	Degree-4 flat-foldable	Exact		NP
All creases	Degree-4 flat-foldable	Finite precision	Weakly NP-hard	NP

Table 1: Summary of our results.

Rigid foldability using all creases: A crease pattern is *rigidly foldable using all creases* if there is a rigid folding motion such that the fold angle at every crease strictly changes (increases or decreases) throughout the entire motion.

For example, the single-vertex crease pattern in Figure 1, left, can be rigidly folded along the line of two creases (leaving two creases unfolded), but also in a different mode that folds along all four creases. Thus it is rigidly foldable using all creases. On the other hand, the single vertex with four perpendicular lines in Figure 1, right, can rigidly fold along either a vertical or horizontal line, but cannot fold using all four creases. So it is rigidly foldable with optional creases, but not using all creases.

Abel et al. [1] gave a simple and efficiently checkable necessary and sufficient condition for single-vertex rigid foldability using all creases. The conjunction of this single-vertex condition locally at every vertex in a general crease pattern leads to a necessary but, sadly, insufficient condition for general rigid foldability: as we will see, the combination of multiple vertices induces a global constraint system of folding speeds.

In this paper, we prove one NP-completeness result and one NP-hardness result about deciding rigid foldability of a general crease pattern in the two models described above; refer to Table 1. First, for the special case of degree-4 flat-foldable crease patterns, we prove in Section 2 that both rigid foldability problems are in NP, even in newly introduced *finite-precision* variations where we ask for an "approximate" rigid folding motion (up to some error/accuracy ε, and assuming zero-thickness paper). Next, we show in Section 3 that deciding finite-precision rigid foldability of a given degree-4 flat-foldable crease pattern using all creases is weakly NP-hard, by a reduction from Partition, and thus weakly NP-complete. Finally, we show that deciding (exact) rigid foldability with optional creases is strongly NP-hard, by a reduction from Positive 1-in-E3 SAT in Section 4. Unlike flat foldability whose complexity [5, 3] originates from the difficulty of layer ordering and possible self-intersection of the material, we show that rigid foldability is hard even for small motions from a planar state where there is no potential self-intersection. Rather, the complexity of rigid foldability comes from the combinatorial behavior of the different possible rigid folding configurations at each vertex (such as the two modes in each of Figure 1, left and right).

Our results help explain why it is harder to fold from an unfolded sheet of material than to unfold a folded state back to a plane, a problem frequently encountered when realizing rigid folding systems such as self-folding matter and reconfigurable robots [27, 16]. Real-world folding systems face the challenge of how to actually execute a specific rigid folding motion, as the flat state in particular is a singular point in the configuration

space having multiple incident rigid folding motions [30]. Usually these folded states are distinguished by different mountain–valley and mode assignments; our results show that finding even one valid such assignment is computationally intractable.

2 Rigid Origami Basics

Before diving into our hardness results, we start with basic definitions and simple results for rigid origami.

2.1 Mathematical Model

First we define a formal model of rigid folding, using the standard concept of isometric foldings as introduced by Robertson [25]; see also [11]. For simplicity, our definitions allow self-intersection (which cannot occur in small foldings from an unfolded state).

Definition 2.1 (Crease Pattern and Isometric Folding)**.** Given a manifold M with or without boundary (representing the material, e.g., $M \subseteq \mathbb{R}^2$), a *crease pattern* is a set $\mathcal{C} \subset M$ partitioning M into a finite cell complex. Given two manifolds M, N with or without boundary (e.g., $N = \mathbb{R}^3$), an *isometric folding* (or *folded state*) is a piecewise-differentiable function $f : M \to N$ if f maps any curve in M to an equal-length curve in N. Such an isometric folding is necessarily continuous. If $\dim M = \dim N = 2$, we call f a *flat folding* (although higher dimensions for $\dim M = \dim N$ are possible; see [25]). Any isometric folding f defines the set $C(f) \subseteq M$ of points where f is not differentiable; assuming f is finitely-piecewise differentiable, $C(f)$ is a crease pattern called the *folded crease pattern of* f. We call f a *folding of* $\mathcal{C}$ if $C(f) \subseteq \mathcal{C}$.

Definition 2.2 (Rigid Origami Folded State)**.** Let $f : M \to \mathbb{R}^3$ be an isometric folding where $M \subset \mathbb{R}^2$ is a closed polygon (representing the sheet of material) and the folded crease pattern $C(f)$ is a planar straight-line finite graph embedded on M. If each 2-cell of $C(f)$ maps via f to a polygon in $\mathbb{R}^3$, then we call f a *rigid origami folded state*.

Let $\mathcal{C} \supseteq C(f)$ be a crease pattern on M. We call f a rigid origami folded state *of* $\mathcal{C}$. Each interior 1-cell c_i of $\mathcal{C}$ is called a *crease line*, and its *fold angle* ρ_i is the signed angle between the normal vectors of the two polygons to which f maps the two 2-cells incident to c_i. We call c_i a *valley* (respectively *mountain*) crease if $\rho_i > 0$ (respectively $\rho_i < 0$). The information of which creases are mountain (M) and which are valley (V) can be thought of as a mapping from the crease lines to the set $\{\mathrm{M}, \mathrm{V}, 0\}$, which is called the *mountain–valley assignment* of the rigid origami folding. The label "0" is reserved for the case of *optional creases* which have a fold angle of $\rho_i = 0$.

Let $\mathbf{R}_{c_i}(\rho_i)$ denote the rotation matrix in $\mathbb{R}^3$ about a crease line $c_i \in \mathcal{C}$ by angle ρ_i if we imagine M to be embedded in the xy plane of $\mathbb{R}^3$. Now let γ be any simple, closed, vertex-avoiding curve drawn on M that crosses, in order, the crease lines $c_1, c_2, \ldots, c_n$ in $\mathcal{C}$. A necessary condition for f to be a rigid origami folding is

$$\mathbf{R}_{c_1}(\rho_1)\mathbf{R}_{c_2}(\rho_2)\cdots\mathbf{R}_{c_n}(\rho_n) = \mathbf{I} \tag{1}$$

for all such curves γ (see [4]). In fact, this condition is also sufficient [20].

Definition 2.3 (Rigid Folding Motion and Configuration Space)**.** A *rigid folding motion* of a crease pattern $\mathcal{C}$ is a continuous function (homotopy) $F : M \times [0,1] \to \mathbb{R}^3$ such that, for any fixed $t \in [0,1]$, the map $f_t : M \to \mathbb{R}^3$ defined by $f_t(x) = F(x,t)$ is a rigid origami folded state of $\mathcal{C}$. We call F a rigid folding motion *from* f_0 *to* f_1.

Equivalently, a rigid folding motion of $\mathcal{C}$ is a path in the *configuration space* consisting of all rigid origami folded states of $\mathcal{C}$. Fixing one 2-cell of $\mathcal{C}$ in $\mathbb{R}^3$ to prevent global translation and rotation, the configuration space can be parameterized by the vector $\mathbf{v}$ of fold angles of the crease lines of $\mathcal{C}$.

2.2 Computational Model

To formally state the computational problems we consider, we need to deal with the limitation of digital computers which cannot exactly represent real numbers. Thus, we need to specify a finite digital representation of crease patterns, and we may need to tolerate some error in deciding whether a rigid motion is actually valid. For now, we define exact versions of the problems (with no error), and leave approximate versions for Definition 2.11.

Definition 2.4 (Rigid Foldability from Flat State)**.** We define two decision problems. In both cases, we are given a straight-line planar graph drawing G on a polygon $M \subset \mathbb{R}^2$, where all vertex coordinates are specified by rational numbers.

1. *Rigid foldability using all creases*: Is there a rigid folding motion from the trivial (unfolded) folding f = identity to an isometric folding $g : M \to \mathbb{R}^3$ ($f \neq g$) whose homotopy H_t satisfies $C(H_t) = G$ for all $t \in (0,1]$ and every fold angle of the crease is strictly increasing or strictly decreasing?
2. *Rigid foldability with optional creases*: Is there a nonempty subset $G' \subset G$ with a positive ("yes") answer to the rigid foldability problem using all creases in G'?

2.3 Degree-4 Flat-Foldable Vertex

The building block of our constructions is the *degree-4 flat-foldable vertex*, a crease-pattern vertex with four creases c_i ($i = 0, 1, 2, 3 \mod 4$) in counterclockwise order with supplementary opposite sector angles, i.e.,

$$(\theta_{0,1}, \theta_{1,2}, \theta_{2,3}, \theta_{3,0}) = (\alpha, \beta, \pi - \alpha, \pi - \beta)$$

($0 < \alpha, \beta < \pi$) where $\theta_{i,i+1}$ is the sector angle between creases c_i and c_{i+1}. Recall that ρ_i denotes the fold angle of crease c_i. The supplementary opposite sector angles satisfy Kawasaki's Theorem [22] and thus the vertex is flat-foldable, meaning that it has a folded state where the fold angles of the creases are all $\pm\pi$.

This type of origami vertex is known to satisfy the interesting and useful property that tangent of half fold angles $\tan \frac{\rho_i}{2} = t_i$ are proportional to each other [7, 17, 12, 28]. Since this result is fundamental to our main result, we present an explicit proof not given in the references.

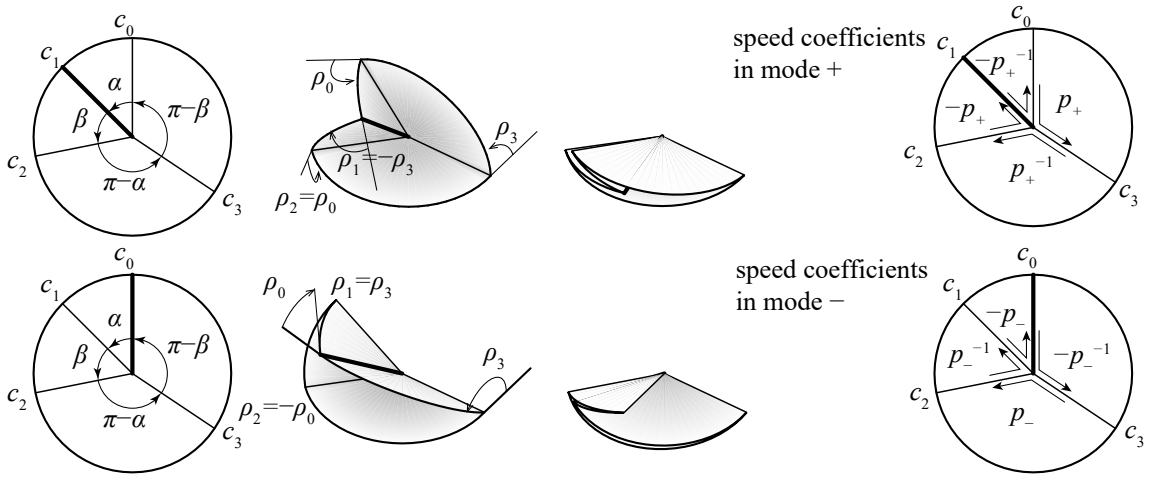

Figure 2: Kinematics of degree-4 flat-foldable vertex. Note that a single vertex has two modes of one-DOF motions (+) and (−).

Theorem 2.5. *Any degree-4 flat-foldable vertex is rigidly foldable. The configuration space of such a vertex, represented by the tangent of half the fold angles, i.e,* $t_i = \tan(\frac{\rho_i}{2})$*, is the union of configurations satisfying:*

$$(t_0, t_1, t_2, t_3) = \begin{cases} (t, -tp_+, t, tp_+) & (\text{“mode +”}), \\ (-tp_-, t, tp_-, t) & (\text{“mode −”}), \end{cases} \tag{2}$$

where $t \in [-\infty, \infty]$ *and* p_+ *and* p_- *are constants defined by*

$$p_+ = p_+(\alpha, \beta) = \frac{1 - \tan\frac{\alpha}{2}\tan\frac{\beta}{2}}{1 + \tan\frac{\alpha}{2}\tan\frac{\beta}{2}}, \tag{3}$$

$$p_- = p_-(\alpha, \beta) = \frac{\tan\frac{\beta}{2} - \tan\frac{\alpha}{2}}{\tan\frac{\beta}{2} + \tan\frac{\alpha}{2}}. \tag{4}$$

Figure 2 shows modes + and −. Note that $0 \le |p_+| < 1$ and $0 \le |p_-| < 1$. Also, if α is strictly smaller than other sector angles, $0 < p_+ < 1$ and $0 < p_- < 1$.

To prove Theorem 2.5, we use the following lemma:

Lemma 2.6. *The fold angles of a degree-4 flat-foldable vertex must satisfy*

$$(\rho_0 = \rho_2 \text{ and } \rho_1 = -\rho_3) \quad \text{or} \quad (\rho_1 = \rho_3 \text{ and } \rho_0 = -\rho_2).$$

Lemma 2.6 can be proven using the spherical law of cosines on the spherical polygon that the rigidly folded vertex cuts out of a sphere of radius 1 with the degree-4 vertex at its center. (The spherical polygon needs to be triangulated by drawing a geodesic between the corners made by c_1 and c_3. See [17, 18] for details.)

Proof of Theorem 2.5. It is straightforward to verify that the fold angles given in Equation (2) verify the rigid foldability condition in Equation (1), thus proving sufficiency of the Theorem 2.5 conditions to rigidly fold a degree-4 flat-foldable vertex.

To prove necessity, suppose we have a rigidly-folded state of the vertex. Assume that in the unfolded state our vertex is at the origin, the material lies in the xy plane in $\mathbb{R}^3$, and c_3 lies on the x-axis with c_0, c_1, and c_2 proceeding counterclockwise from there. If we folded the vertex into our given rigid state while leaving the sector between c_2 and c_3 fixed in the xy plane, then we may consecutively rotate each sector angle through, and each fold angle around, the positive x-axis to obtain a matrix equation as follows: Let $\mathbf{R}_x(\theta)$ and $\mathbf{R}_z(\theta)$ denote the rotation matrices about the x- and z-axes by θ, respectively, i.e.,

$$\mathbf{R}_x(\theta) := \begin{bmatrix} 1 & 0 & 0 \\ 0 & \cos\theta & -\sin\theta \\ 0 & \sin\theta & \cos\theta \end{bmatrix} \text{ and } \mathbf{R}_z(\theta) := \begin{bmatrix} \cos\theta & -\sin\theta & 0 \\ \sin\theta & \cos\theta & 0 \\ 0 & 0 & 1 \end{bmatrix}.$$

Then we have

$$\mathbf{R}_z(\pi-\beta)\mathbf{R}_x(\rho_0)\mathbf{R}_z(\alpha)\mathbf{R}_x(\rho_1)\mathbf{R}_z(\beta)\mathbf{R}_x(\rho_2)\mathbf{R}_z(\pi-\alpha)\mathbf{R}_x(\rho_3) = \mathbf{I}.$$

We employ Lemma 2.6 and bring some matrices to the other side to obtain

$$\mathbf{R}_z(\pi-\beta)\mathbf{R}_x(\rho_2)\mathbf{R}_z(\alpha)\mathbf{R}_x(-\rho_3) = \mathbf{R}_x(-\rho_3)\mathbf{R}_z(-(\pi-\alpha))\mathbf{R}_x(-\rho_2)\mathbf{R}_z(-\beta).$$

The 1st row, 2nd column entry of this matrix equation simplifies to

$$(\cos\rho_2 - \cos\rho_3)\sin\alpha\cos\beta + (\cos\rho_2\cos\rho_3 - 1)\cos\alpha\sin\beta + \sin\rho_2\sin\rho_3\sin\beta = 0.$$

Recall that $t_i = \tan(\rho_i/2)$, which means that

$$\sin\rho_i = \frac{2t_i}{1+t_i^2} \text{ and } \cos\rho_i = \frac{1-t_i^2}{1+t_i^2}.$$

Substituting these into our condition and simplifying a bit we obtain

$$\frac{t_2^2-t_3^2}{(1+t_2^2)(1+t_3^2)}\sin\alpha\cos\beta + \frac{t_2^2+t_3^2}{(1+t_2^2)(1+t_3^2)}\cos\alpha\sin\beta - \frac{2t_2t_3}{(1+t_2^2)(1+t_3^2)}\sin\beta = 0.$$

Multiplying both sides by $(1+t_2^2)(1+t_3^2)$ and re-arranging further we get

$$2\sin\beta\frac{t_3}{t_2} = \left(1-\left(\frac{t_3}{t_2}\right)^2\right)\sin\alpha\cos\beta + \left(1+\left(\frac{t_3}{t_2}\right)^2\right)\cos\alpha\sin\beta,$$

from which we solve for t_3/t_2 to obtain two solutions:

$$\frac{t_3}{t_2} = \frac{\cos\left(\frac{\alpha+\beta}{2}\right)}{\cos\left(\frac{\alpha-\beta}{2}\right)} = \frac{1-\tan\frac{\alpha}{2}\tan\frac{\beta}{2}}{1+\tan\frac{\alpha}{2}\tan\frac{\beta}{2}} \text{ and } \frac{t_2}{t_3} = -\frac{\sin\left(\frac{\alpha+\beta}{2}\right)}{\sin\left(\frac{\alpha-\beta}{2}\right)} = \frac{\tan\frac{\beta}{2}-\tan\frac{\alpha}{2}}{\tan\frac{\beta}{2}+\tan\frac{\alpha}{2}}.$$

Thus the fold angles of our rigidly folded state satisfy the Equation (2) formulas, where Lemma 2.6 verifies that the mountain and valley creases must match one of the two modes shown in Figure 2. □

Theorem 2.5 implies that the fold angles of a degree-4 flat-foldable vertex are proportional to each other when parameterized by the tangent of the half angle. Also, the configuration space curves determined by Equation (2) share exactly one configuration point $t_0 = t_1 = t_2 = t_3 = 0$ (the flat state). At this point the configuration space branches to two rigid folding modes, each of which is one-DOF. We can determine the folding motion of the vertex by specifying the mode and the fold angle of one of the creases.

Definition 2.7 (Speed coefficient)**.** For a pair of incident creases c_i and c_j, we call $p(i,j) := \tan\frac{\rho_i}{2} / \tan\frac{\rho_j}{2}$ the *speed coefficient* from c_j to c_i.

The speed coefficients are also known as the *fold-angle multipliers* [12]. The choice of modes + and − in Equation (2) (called the *mode assignment*) determine the speed coefficients between creases:

$$(p(0,1), p(1,2), p(2,3), p(3,0)) = \begin{cases} (-p_+^{-1}, -p_+, p_+^{-1}, p_+) & \text{in mode } +, \\ (-p_-, p_-^{-1}, p_-, -p_-^{-1}) & \text{in mode } -. \end{cases} \tag{5}$$

In the special case of $\beta = 90°$, the speed coefficients can be written using a single variable:

$$(p(0,1), p(1,2), p(2,3), p(3,0)) = \begin{cases} (-p^{-1}, -p, p^{-1}, p) & \text{in mode } +, \\ (-p, p^{-1}, p, -p^{-1}) & \text{in mode } -. \end{cases} \tag{6}$$
$$\text{where} \quad p = p(\alpha) = p_+(\alpha, 90°) = p_-(\alpha, 90°) = \frac{1 - \tan\frac{\alpha}{2}}{1 + \tan\frac{\alpha}{2}}.$$

In particular, if we chose $\alpha = \arctan\frac{3}{4}$, then we obtain $p = \frac{1}{2}$. We will use this setting in Section 4.

In another special case, $\alpha = \beta$, the speed coefficient can again be written using single variable:

$$(p(0,1), p(1,2), p(2,3), p(3,0)) = \begin{cases} (-p^{-1}, -p, p^{-1}, p) & \text{in mode } +, \\ (0, \infty, 0, -\infty) & \text{in mode } -, \end{cases} \tag{7}$$
$$\text{where} \quad p = p_+(\alpha, \alpha) = \frac{1 - \tan^2\frac{\alpha}{2}}{1 + \tan^2\frac{\alpha}{2}} = \cos\alpha \quad \text{and} \quad p_-(\alpha, \alpha) = 0.$$

Theorem 2.5 gives us a continuously parameterized family of rigid origami foldings for degree-4 flat-foldable vertices. Thus we have the following:

Lemma 2.8. *A degree-4 flat-foldable vertex has exactly four mountain–valley assignments (allowing* 0 *assignment to denote an unfolded crease) that are* valid *in the sense that there is a rigid folding motion from the flat state consistent with the mountain–valley assignment. Furthermore, each valid mountain–valley assignment restricts the configuration space to a unique* 1*-parameter curve, i.e.,* 1*-DOF mechanism, having uniquely determined speed coefficients between incident edges, which we call the speed coefficients* induced *by the valid mountain–valley assignment.*

Proof. The two binary options, (1) choice of modes + and − and (2) the sign of t, give four folding paths, along which the signs of fold angles (assignment) are unchanged by Equation (2). The opposite paths in the same mode have reversed mountain–valley assignments from each other, and the paths in different modes have different assignments because edges 0 and 3 have the same (nonzero) assignment in mode + and the opposite assignment in mode −. So, each mountain–valley assignment gives a unique 1-parameter folding path in the configuration space. □

2.4 Assembly: Degree-4 Flat-Foldable Origami

We call a crease pattern composed solely of degree-4 flat-foldable vertices a *degree-4 flat-foldable mesh*. (Such a mesh is really only locally flat-foldable.) For our hardness proof of rigid origami, we will use a degree-4 flat-foldable mesh with optional creases. Determining the rigid foldability of degree-4 flat-foldable meshes is a problem of assigning modes + or − for each vertex in such a way that the folding speeds of the creases will not be in conflict. Note that because we are only interested in rigidly folding our crease pattern a finite amount from the flat, unfolded state, we do not need to worry about the possibility of different parts of the material colliding or self-intersecting.

The following directly follows from Lemma 2.8 and the definition of speed coefficients. (See also [12].)

Corollary 2.9 (Assignment Problem)**.** *For a mountain–valley assignment of a degree-4 flat-foldable mesh, there is at most one folding path that forms a 1-manifold in the configuration space.*

Corollary 2.10 (Closure Condition)**.** *A mountain–valley assignment of degree-4 flat-foldable mesh yields a rigid folding motion if and only if*

1. *for each vertex v, the mountain–valley assignment of the creases incident to v is valid (according to Lemma 2.8);*
2. *for each k-gonal face surrounded by creases $c_0, c_1, \ldots, c_{k-1}$ (in cyclic order), the speed coefficients $p_i = p(c_{i+1}, c_i)$ induced by the mountain–valley assignment at the shared vertex between c_i and c_{i+1} (according to Lemma 2.8) satisfy the following:*

$$\prod_{i=0,1,\ldots,k-1} p_i = 1. \tag{8}$$

Equation (8) provides a natural metric for measuring error in a candidate rigid folding motion.

Definition 2.11 (Finite-Precision Degree-4 Flat-Foldable Rigid Foldability)**.** As in Definition 2.4, we define two decision problems whose primary input is a straight-line planar graph drawing G on a polygon $M \subset \mathbb{R}^2$, where all vertex coordinates are specified by rational numbers. Now G is constrained to have all vertices be degree-4 flat-foldable and we have an additional input $\varepsilon > 0$ (specified as a rational number).

1. *Rigid foldability using all creases*: Is there a mountain–valley assignment whose induced fold-angle multipliers satisfy, at each vertex,

$$\prod_{i=0,1,\ldots,k-1} p_i \in [1-\varepsilon, 1+\varepsilon]? \tag{9}$$

2. *Rigid foldability with optional creases*: Is there a nonempty subset $G' \subset G$ with a positive ("yes") answer to the finite-precision rigid foldability problem using all creases in G'?

Theorem 2.12 (Finite-Precision Rigid Foldability is in NP)**.** *Both finite-precision degree-4 flat-foldable rigid foldability problems are in* NP*, even with $\varepsilon = 0$ (exact precision).*

Proof. First observe that we can confirm that the given crease pattern is flat foldable in P. At each vertex $\mathbf{u}$ with neighbors $\mathbf{v}_1, \mathbf{v}_2, \mathbf{v}_3, \mathbf{v}_4$, we reflect $\mathbf{v}_1 - \mathbf{u}$ through $\mathbf{v}_i - \mathbf{u}$ for $i \in \{2, 3, 4\}$, and then verify that the resulting vector is identical to $\mathbf{v}_1 - \mathbf{u}$. Here we use that the reflection $\mathbf{p}'$ of vector $\mathbf{p}$ through another vector $\mathbf{q}$ can be done with $O(1)$ additions, multiplications, and divisions:

$$\mathbf{p}' = \mathbf{p} - 2\frac{(\mathbf{p}\cdot\mathbf{q}^\perp)\mathbf{q}^\perp}{\mathbf{q}\cdot\mathbf{q}}, \quad \text{where} \quad (x,y)^\perp = (-y,x). \tag{10}$$

Next we nondeterministically guess the mountain–valley assignment and, for the optional-crease problem, the subset G' of creases.

It remains to verify Inequality (9) at each vertex. Equations (3) and (4) represent each p_i term in the product as a rational function of tangents of half-angles. Recall the tangent half-angle formula:

$$\tan\tfrac{\theta}{2} = \csc\theta - \cot\theta.$$

The latter trigonometric functions can be represented by radical expressions on the vertex coordinates, specifically, their absolute difference in x coordinates, their absolute difference in y coordinates, and their Euclidean distance (which involves a square root). Therefore the product of the p_i's at a vertex can be represented as a constant-complexity expression involving addition, subtraction, multiplication, division, and square roots on the input rationals. Comparing such an expression to $1 \pm \varepsilon$ (even with $\varepsilon = 0$) can be done exactly in polynomial time; see, e.g., [8]. □

Note that rigid foldability of general origami with non-degree-4 or non-flat-fordable vertices may not be in NP.

2.5 Square Twist Fold

Next we show a classic example of rigid folding, which we will use in our gadgets in Section 4. Specifically, by combining four degree-4 flat-foldable vertices, we may obtain a rigid folding version of the "square twist fold" with arbitrary minimum sector angle α (Figure 3). Unlike the original square twist fold [13, 18], we choose the mountain–valley assignment to allow rigid foldability. Such a system can fold in two ways if we take the symmetry into account [12, 30].

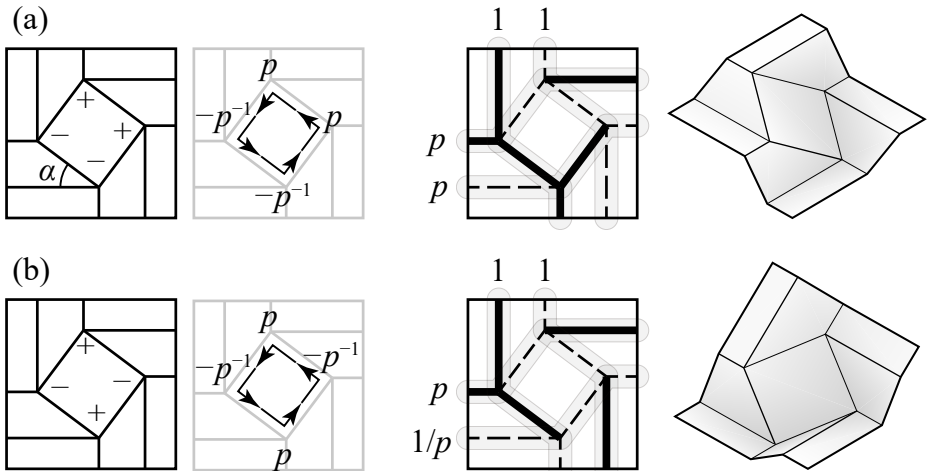

Figure 3: Two different modes (a) and (b) of a square twist with minimum sector angle α. The left two columns show the assignment of modes + and − to obtain the consistent loop, which gives the mountain–valley assignments in the third column, which fold to the 3D state in the fourth column. The numbers 1, p, $1/p$ represents the absolute folding speeds measured in tangent of half of fold angles of edges along the chain of opposite edges.

Lemma 2.13. *There are only four mountain–valley assignments and thus two modes (up to symmetry) that allow the square twist to fold rigidly, for any minimum sector angle α. They are the ones shown in Figure 3 along with the relative folding speed coefficients of the creases on the boundary.*

Proof. Consider the central square composed of creases c_0, c_1, c_2, c_3. The problem of determining mountain–valley assignments is equivalent to assigning the speed coefficients

$$p(c_{i+1}, c_i) = \begin{cases} p(\alpha) & \text{mode } +, \\ -\frac{1}{p(\alpha)} & \text{mode } -, \end{cases}$$

where $p(\alpha)$ is defined by Equation (6). Equation (8) is satisfied if and only if the number of mode +'s is 2. The possible pattern is either $++--$ or $+-+-$ up to symmetry, as shown in Figure 3. □

3 Rigid Foldability using All Creases is Weakly NP-hard

Theorem 3.1. *Finite-precision degree-4 flat-foldable rigid foldability using all the creases is weakly* NP*-complete.*

To prove this theorem, we reduce from *Partition*: given a multiset $A = \{a_1, a_2, \ldots, a_n\}$ of n positive integers, is there a subset $S \subseteq A$ that partitions the elements into two halves of equal sum, i.e., $\Sigma(S) = \sum(A \setminus S) = \frac{1}{2}\Sigma(A)$, where $\Sigma(S) = \sum_{x \in S} x$. This problem is known to be weakly NP-hard [14, 21].

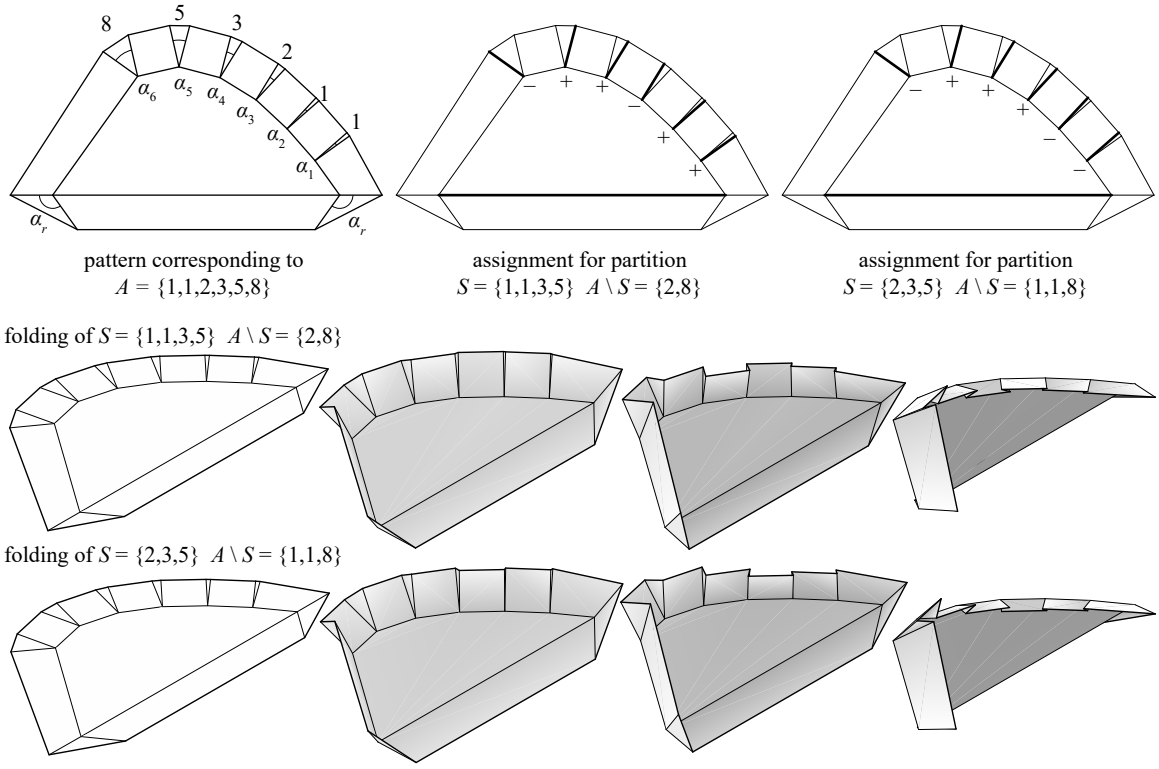

Figure 4: Rigid origami realizing a given Partition instance with $n > 4$ integers by an $(n+2)$-gonal closed chain of degree-4 flat-foldable vertices. The sector angles α_i of n consecutive vertices are designed from the set of integers, and two vertices form mirror-symmetric degree-4 vertices (top-left). Partitioning corresponds to a mountain–valley assignment for each vertex (top-middle and top-right). The pattern is rigidly foldable when the mountain–valley pattern partitions the set into equal sums (middle and bottom rows).

Proof. Theorem 2.12 establishes membership in NP. To demonstrate the main idea in our NP-hardness reduction, we first pretend that we can compute the needed real values exactly, and second we take care of finite precision.

Consider a Partition instance $A = \{a_1, a_2, \ldots, a_n\}$ where $n > 4$. We construct a crease pattern of an $(n+2)$-gonal closed chain of degree-4 flat-foldable vertices $\mathbf{v}_0, \mathbf{v}_1, \ldots, \mathbf{v}_{n+1}$; refer to Figure 4. We start with n consecutive flat-foldable vertices $\mathbf{v}_1, \mathbf{v}_2, \ldots, \mathbf{v}_n$ where $\mathbf{v}_i$ has $\alpha = \alpha_i \in (0°, 90°)$ and $\beta = 90°$, so that $\sum_i \alpha_i < 360°$. We split the remaining angle $360° - \sum_i \alpha_i$ into halves, and make the last two vertices $\mathbf{v}_0$ and $\mathbf{v}_{n+1}$ be mirror symmetric and flat-foldable with $\alpha = \beta = \alpha_r = (360° - \sum_i \alpha_i)/2$.

Now we consider the speed coefficients in a rigid folding. For $1 \le i \le n$, by Equation (6), vertex $\mathbf{v}_i$ has a speed coefficient of $p_i = p(\alpha_i) = \frac{1-\tan\frac{\alpha_i}{2}}{1+\tan\frac{\alpha_i}{2}}$ (mode +) or p_i^{-1} (mode −). Because $\alpha_i \in (0, 90°)$, $\tan\frac{\alpha_i}{2} \in (0, 1)$, so p_i and p_i^{-1} are positive, meaning that the creases $\mathbf{v}_i\mathbf{v}_{i+1}$ for $0 \le i \le n$ all have the same mountain–valley assignment. By Equation (7), vertex $\mathbf{v}_{n+1}$ has a speed coefficient of $p_r = p(\alpha_r, \alpha_r) = \frac{1-\tan^2\frac{\alpha_r}{2}}{1+\tan^2\frac{\alpha_r}{2}}$ (mode +) and ∞ (mode −), and

vertex $\mathbf{v}_0$ has speed coefficient of 0 (mode +) and p_r^{-1} (mode −). In order that all creases of vertices $\mathbf{v}_{n+1}$ and $\mathbf{v}_0$ fold simultaneously, $\mathbf{v}_{n+1}$ must chose mode + and $\mathbf{v}_0$ must chose mode −, because p_r is nonzero and finite.

Now we tweak α_i properly so that choosing the vertices that folds in mode − is equivalent to choosing the element of S from A, and the closure constraint (Equation (8)) is equivalent to the Partition problem. Specifically, we set the variables α_i such that

$$\frac{a_i}{\Sigma(A)} = \log p_i^{-1}, \tag{11}$$

for all $i = 1, 2, \ldots, n$, and thus

$$\tan\frac{\alpha_i}{2} = \frac{1-p_i}{1+p_i} = \frac{1-e^{-a_i/\Sigma(A)}}{1+e^{-a_i/\Sigma(A)}} = \tanh\left(\frac{a_i}{2\Sigma(A)}\right). \tag{12}$$

Then, by Equation (8), the formed pattern is rigidly foldable if and only if there exists a subset $S \subset A$ such that

$$\left(\prod_{i\in S} p_i^{-1}\right)\left(\prod_{i\in A\setminus S} p_i\right) p_r p_r^{-1} = 1, \tag{13}$$

which, by taking the logarithm on both sides and multiplying by $\Sigma(A)$, is equivalent to the given Partition problem:

$$\Sigma(S) - \Sigma(A \setminus S) = 0. \tag{14}$$

Now we show that the ranges of α_i and α_r are valid. Plugging in Equation (12), we have

$$\sum_i \alpha_i = \sum_i 2\arctan\left(\tanh\left(\frac{a_i}{2\Sigma(A)}\right)\right). \tag{15}$$

Because $\frac{a_i}{2\Sigma(A)} \in [0, \frac{1}{2}]$, we have

$$\arctan\tanh\frac{a_i}{2\Sigma(A)} \in \left(0.86\,\frac{a_i}{2\Sigma(A)}, \frac{a_i}{2\Sigma(A)}\right). \tag{16}$$

Combining the previous two equations, we have

$$\sum_i \alpha_i \in (0.86, 1) \subseteq \left(\tfrac{\pi}{4}, \tfrac{\pi}{3}\right). \tag{17}$$

Thus, $\sum_{i\in\{1,2,\ldots,n\}} \alpha_i \in (45°, 60°)$, so $\alpha_r = (360° - \sum_{i\in\{1,2,\ldots,n\}} \alpha_i)/2 \in (150°, 157.5°)$.

Because $\alpha_j \le \sum_i \alpha_i$, we also obtain $\alpha_j \in (0, 60°)$, and thus the central polygon is convex. Thus we can always construct the $(n+2)$-gon from the slope of each segment derived from these turn angles. By Equation (6), the range on α_j ensures $p_j \in (0.26, 1)$, which will be useful later for avoiding close-to-singular vertices. By Equation (7), the range $\alpha_r \in (150°, 157.5°)$ ensures that $p_r \in (-0.93, -0.86)$, in particular, nonzero and finite, proving the assumption.

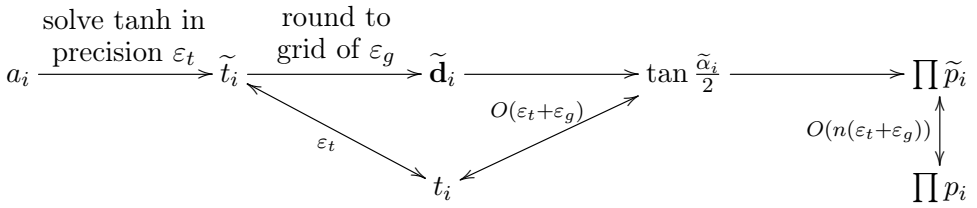

Figure 5: Sequence of rational approximations to the exact construction and their dependencies. In general, $\widetilde{x}$ denotes a computed approximation to the quantity x, and a quantity ε on an arrow denotes an absolute error bound of $|\widetilde{x} - x| \leq \varepsilon$.

The rest of the proof addresses the requirement that the reduction must be computed in polynomial time — i.e., $(n \log \Sigma(A))^{O(1)}$ time — using finite precision, not arbitrary real numbers. We will follow the exact construction above, but using rational approximations to the relevant values. Figure 5 shows the sequence of approximations we will now describe.

The reduction algorithm first computes $\widetilde{t}_i$, an approximation to $t_i = \tan \frac{\alpha_i}{2}$ given by Equation (12), but with precision ε_t, i.e., $|\widetilde{t}_i - t_i| \leq \varepsilon_t$, as follows. Specifically, we set $\varepsilon_t = \frac{1}{3cn\Sigma(A)}$ for a constant $c \geq 1$ defined below. We can compute each $x = \frac{a_i}{2\Sigma(A)}$ exactly, represented as a rational. Then we approximate $\tanh x = \frac{e^{2x}-1}{e^{2x}+1} = 1 - \frac{2}{e^{2x}+1}$ to within $\pm\varepsilon_t$ as follows. First we compute e^{2x} to within $\pm\varepsilon_t$, i.e., obtain a rational approximation $\widetilde{e^{2x}} \in [e^{2x} - \varepsilon_t, e^{2x} + \varepsilon_t]$. Standard algorithms for approximating e^x can do so in $O(\log\log \frac{1}{\varepsilon_t})$ multiplications on $O(\log \frac{1}{\varepsilon_t})$-bit integers [6], each of which can be done naively in $O(\log^2 \frac{1}{\varepsilon_t})$ time or using the recent $O(\log \frac{1}{\varepsilon_t} \log\log \frac{1}{\varepsilon_t})$ algorithm [15], for a total of $\log^{O(1)} \frac{1}{\varepsilon_t} = \log^{O(1)} n\Sigma(A)$ time (and thus polynomial time). Given $\widetilde{e^{2x}}$, we can compute $\widetilde{\tanh x}$ and $\widetilde{t}_i$ exactly using rational arithmetic, with total error given by

$$\begin{aligned}
\widetilde{t}_i - t_i &= \left(1 - \frac{2}{\widetilde{e^{2x}} + 1}\right) - \left(1 - \frac{2}{e^{2x}+1}\right) \\
&\in \left[\left(-\frac{2}{(e^{2x}+1-\varepsilon_t)} + \frac{2}{(e^{2x}+1)}\right), \left(-\frac{2}{(e^{2x}+1+\varepsilon_t)} + \frac{2}{(e^{2x}+1)}\right)\right] \\
&= \left[\frac{-2\varepsilon_t}{(e^{2x}+1)(e^{2x}+1-\varepsilon_t)}, \frac{2\varepsilon_t}{(e^{2x}+1)(e^{2x}+1+\varepsilon_t)}\right].
\end{aligned}$$

Using $e^{2x} > 1$ and $\varepsilon_t \in (0,1)$, we can bound the error to show that $\widetilde{t}_i \in (t_i - \varepsilon_t, t_i + \varepsilon_t)$:

$$\begin{aligned}
\frac{2\varepsilon_t}{(e^{2x}+1)(e^{2x}+1-\varepsilon_t)} &< \frac{2\varepsilon_t}{2(2-\varepsilon_t)} < \frac{2\varepsilon_t}{2} = \varepsilon_t, \\
\frac{2\varepsilon_t}{(e^{2x}+1)(e^{2x}+1+\varepsilon_t)} &< \frac{2\varepsilon_t}{2(2+\varepsilon_t)} < \frac{2\varepsilon_t}{4} < \varepsilon_t.
\end{aligned}$$

Next the algorithm computes an approximation of the crease pattern, one vertex at a time, with computed vertex $\widetilde{\mathbf{v}}_i$ approximating the ideal vertex $\mathbf{v}_i$. Refer to Figure 6. Vertices $\widetilde{\mathbf{v}}_0, \widetilde{\mathbf{v}}_1, \ldots, \widetilde{\mathbf{v}}_n$ will lie on a grid with resolution $\varepsilon_g = \varepsilon_t = \frac{1}{3cn\Sigma(A)}$. First we compute

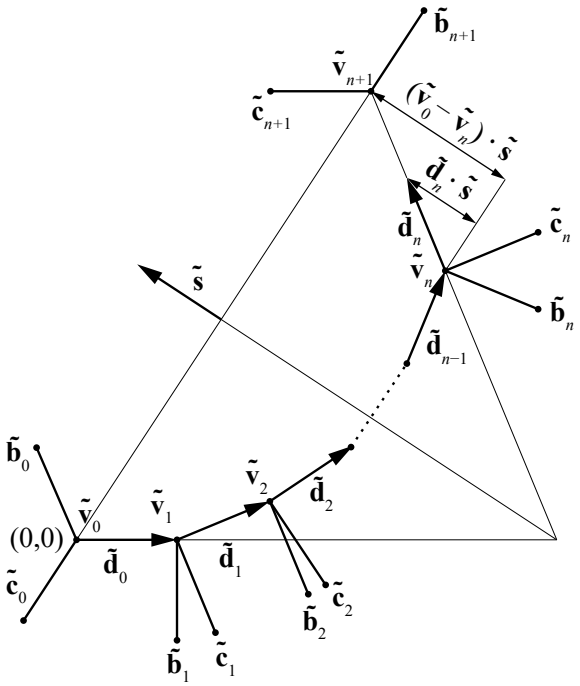

Figure 6: The actual construction step of rigid origami realizing the Partition problem.

difference vectors $\widetilde{\mathbf{d}}_i$ for $0 \le i \le n$, whose coordinates are also multiples of ε_g. For $i < n$, $\widetilde{\mathbf{d}}_i$ corresponds to $\widetilde{\mathbf{v}}_{i+1} - \widetilde{\mathbf{v}}_i$ (but $i = n$ will behave slightly differently), so we can compute $\widetilde{\mathbf{v}}_i$ for $1 \le i \le n$ via $\widetilde{\mathbf{v}}_{i+1} = \widetilde{\mathbf{v}}_i + \widetilde{\mathbf{d}}_i$, using $\widetilde{\mathbf{v}}_0 = (0,0)$ as a base case. We define $\widetilde{\mathbf{d}}_0 = (1,0)$, the unit rightward vector. Given $\widetilde{\mathbf{d}}_{i-1}$, we compute $\widetilde{\mathbf{d}}_i$ by rotating the vector $\widetilde{\mathbf{d}}_{i-1}$ by the rotation matrix

$$\begin{pmatrix} \frac{1-\widetilde{t}_i^2}{1+\widetilde{t}_i^2} & \frac{-2\widetilde{t}_i}{1+\widetilde{t}_i^2} \\ \frac{2\widetilde{t}_i}{1+\widetilde{t}_i^2} & \frac{1-\widetilde{t}_i^2}{1+\widetilde{t}_i^2} \end{pmatrix}, \tag{18}$$

and rounding the resulting coordinates to the nearest integer multiples of ε_g. (Note that, while we can compute the coordinates given by Equation (18) exactly, if we do not round them to a common grid in each step, then the bit-length of the numbers will grow exponentially as we compute each $\widetilde{\mathbf{d}}_i$ from the previous.) Finally, we compute $\widetilde{\mathbf{v}}_{n+1}$. We want $\widetilde{\mathbf{v}}_{n+1}$ and $\widetilde{\mathbf{v}}_0$ to be exactly mirror symmetric through the bisecting vector $\widetilde{\mathbf{s}}$ of $\widetilde{\mathbf{d}}_n$ and $-\widetilde{\mathbf{d}}_0$. This bisecting vector is given by $\widetilde{\mathbf{s}} = \frac{1}{2}(\widetilde{\mathbf{d}}_n - \widetilde{\mathbf{d}}_0)$. We check that $\widetilde{\mathbf{v}}_n + \widetilde{\mathbf{d}}_n$ has a smaller dot product than $-\widetilde{\mathbf{v}}_0$ does with the bisecting vector, so that we can make $\widetilde{\mathbf{v}}_{n+1} - \widetilde{\mathbf{v}}_n$ longer than 1 unit. If this condition does not hold, we restart the entire algorithm with the order $a_1, a_2, \ldots, a_n$ reversed. Then we set $\widetilde{\mathbf{v}}_{n+1}$ to

$$\widetilde{\mathbf{v}}_n + \frac{(\widetilde{\mathbf{v}}_0 - \widetilde{\mathbf{v}}_n) \cdot \widetilde{\mathbf{s}}}{\widetilde{\mathbf{d}}_n \cdot \widetilde{\mathbf{s}}}\, \widetilde{\mathbf{d}}_n$$

(which is already on the grid of resolution ε_g, so needs no rounding).

Now we compute the boundary vertices $\widetilde{\mathbf{b}}_i, \widetilde{\mathbf{c}}_i$, connected via creases to $\widetilde{\mathbf{v}}_i$, for each $i = 0, 1, \ldots, n+1$. For $i = 1, 2, \ldots, n$, we use equations $\widetilde{\mathbf{b}}_i - \widetilde{\mathbf{v}}_i = -\widetilde{\mathbf{d}}_{i-1}^{\perp}$ and $\widetilde{\mathbf{c}}_i - \widetilde{\mathbf{v}}_i = -\widetilde{\mathbf{d}}_i^{\perp}$ (i.e., 90° right rotation of vectors $\widetilde{\mathbf{d}}_{i-1}$ and $\widetilde{\mathbf{d}}_i$), which make $\widetilde{\mathbf{b}}_i$ and $\widetilde{\mathbf{c}}_i$ remain on the grid of resolution ε_g. For $i = 0$ and $i = n+1$, we use an extension of the segment $\widetilde{\mathbf{v}}_0\widetilde{\mathbf{v}}_{n+1}$ to define one boundary vertex, and use reflections to compute the other boundary vertex. Precisely, we define $\widetilde{\mathbf{c}}_0$ and $\widetilde{\mathbf{b}}_{n+1}$ via

$$\widetilde{\mathbf{c}}_0 - \widetilde{\mathbf{v}_0} = \frac{\widetilde{\mathbf{v}}_0 - \widetilde{\mathbf{v}}_{n+1}}{\lceil \|\widetilde{\mathbf{v}}_0 - \widetilde{\mathbf{v}}_{n+1}\| \rceil}, \quad \widetilde{\mathbf{b}}_{n+1} - \widetilde{\mathbf{v}}_{n+1} = \frac{\widetilde{\mathbf{v}}_{n+1} - \widetilde{\mathbf{v}}_0}{\lceil \|\widetilde{\mathbf{v}}_{n+1} - \widetilde{\mathbf{v}}_0\| \rceil};$$

and define $\widetilde{\mathbf{b}}_0$ and $\widetilde{\mathbf{c}}_{n+1}$ via $\widetilde{\mathbf{b}}_0 - \widetilde{\mathbf{v}}_0$ equalling the reflection of $\widetilde{\mathbf{d}}_0$ through $\widetilde{\mathbf{v}}_0\widetilde{\mathbf{v}}_{n+1}$, and $\widetilde{\mathbf{v}}_{n+1} - \widetilde{\mathbf{c}}_{n+1}$ equalling the reflection of $\widetilde{\mathbf{d}}_n$ through $\widetilde{\mathbf{v}}_0\widetilde{\mathbf{v}}_{n+1}$. These coordinates are rational, with numerators and denominators bounded by a polynomial in $1/\varepsilon_g$.

Now we prove a sequence of claims about the constructed crease pattern in order to show it is rigidly foldable up to precision ε.

First we claim that the crease pattern is exactly locally flat foldable. This claim follows by construction: for each vertex $\widetilde{\mathbf{v}}_i$, we constructed $\widetilde{\mathbf{b}}_i$ and $\widetilde{\mathbf{c}}_i$ exactly to guarantee local flat foldability of $\widetilde{\mathbf{v}}_i$. For $i = 1, 2, \ldots, n$, we used 90° rotations to guarantee two right angles; and for $i = 0$ and $i = n+1$, we used exact reflections.

Second we claim that vertices $\widetilde{\mathbf{v}}_0$ and $\widetilde{\mathbf{v}}_{n+1}$ are mirror symmetric with each other, and each have two collinear creases ($\alpha = \beta$), as needed by the Partition reduction. This claim follows from the construction: the exact computation of the bisecting vector $\widetilde{\mathbf{s}}$ and vertices $\widetilde{\mathbf{c}}_0$ and $\widetilde{\mathbf{b}}_{n+1}$. Thus these two vertices contribute $\widetilde{p}_r$ and $\widetilde{p}_r^{-1}$ respectively (for some $\widetilde{p}_r$) to the closure-condition product (8), so they cancel and we can ignore them.

Third we claim that each vertex $\widetilde{\mathbf{v}}_i$, for $1 \le i \le n$, has $\beta = 90°$ (exactly) and $\alpha = \widetilde{\alpha}_i$ satisfying $\tan \frac{\widetilde{\alpha}_i}{2} = \widetilde{t}_i \pm O(\varepsilon_g) = t_i \pm O(\varepsilon_g + \varepsilon_t)$. That $\beta = 90°$ follows from the construction of $\widetilde{\mathbf{b}}_i$ and $\widetilde{\mathbf{c}}_i$. To measure $\widetilde{\alpha}_i$, we first analyze the lengths of $\widetilde{\mathbf{d}}_i$: $\|\widetilde{\mathbf{d}}_0\| = 1$, and $\widetilde{\mathbf{d}}_i$ is an ε_g-grid rounding of a rotation of $\widetilde{\mathbf{d}}_{i+1}$, so $|\,\|\widetilde{\mathbf{d}}_i\| - \|\widetilde{\mathbf{d}}_{i+1}\|\,| \le \frac{1}{\sqrt{2}}\varepsilon_g$, and therefore $\|\widetilde{\mathbf{d}}_i\|$ is within $\pm\frac{n}{\sqrt{2}}\varepsilon_g$ of 1. Because $\varepsilon_g \le \frac{1}{3n\Sigma(A)} < \frac{1}{\sqrt{2}\,n}$, $\|\widetilde{\mathbf{d}}_i\| \ge \frac{1}{2}$. By construction, the angle $\widetilde{\alpha}_i$ at $\widetilde{\mathbf{v}}_i$ is equal to the angle between vectors $\widetilde{\mathbf{d}}_i$ and $\widetilde{\mathbf{d}}_{i-1}$. Because these vectors have length $\ge \frac{1}{2}$, the angle change caused by rounding the rotated $\widetilde{\mathbf{d}}_{i-1}$ is at most $\sqrt{2}\,\varepsilon_g$ (refer to Figure 7), and thus

$$\left| \frac{\widetilde{\alpha}_i}{2} - \arctan \widetilde{t}_i \right| \le \tfrac{1}{\sqrt{2}}\,\varepsilon_g.$$

Now

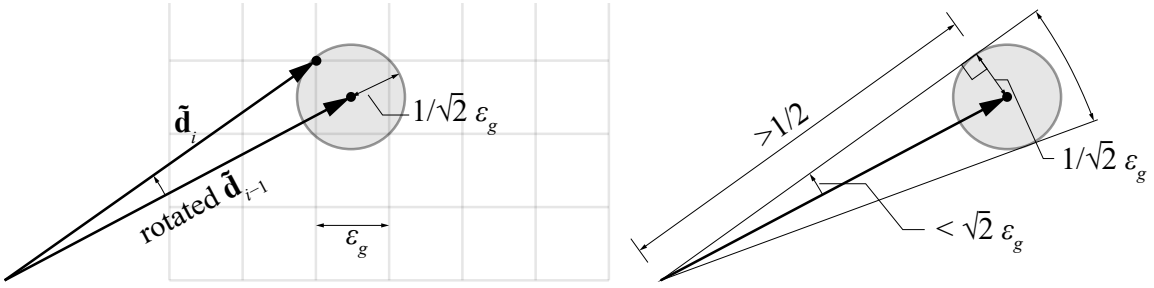

Figure 7: Rounding the end point of $\mathbf{v}_i$ to a grid causing a rotation of at most $\sqrt{2}\varepsilon_g$

$$\begin{aligned}\left|\tan\frac{\widetilde{\alpha}_i}{2}-\widetilde{t}_i\right| &\le \left|\tan\left(\arctan\widetilde{t}_i+\frac{1}{\sqrt{2}}\varepsilon_g\right)-\widetilde{t}_i\right| \\ &= \left|\frac{\widetilde{t}_i+\tan\frac{1}{\sqrt{2}}\varepsilon_g}{1-\widetilde{t}_i\tan\frac{1}{\sqrt{2}}\varepsilon_g}-\widetilde{t}_i\right| \\ &= \left|\frac{(1+\widetilde{t}_i^2)\tan\frac{1}{\sqrt{2}}\varepsilon_g}{1-\widetilde{t}_i\tan\frac{1}{\sqrt{2}}\varepsilon_g}\right| \\ &\le 2(1+\widetilde{t}_i^2)\tan\tfrac{1}{\sqrt{2}}\varepsilon_g,\end{aligned}$$

because we claim that $\widetilde{t}_i\tan\frac{1}{\sqrt{2}}\varepsilon_g \le \frac{1}{2}$. First, because $\alpha_i \in (0, 60°)$, we have $t_i \in (0, \frac{1}{\sqrt{3}})$ and thus $\widetilde{t}_i \in \left(-\varepsilon_t, \frac{1}{\sqrt{3}}+\varepsilon_t\right)$. Then the claim follows:

$$\widetilde{t}_i\tan\tfrac{1}{\sqrt{2}}\varepsilon_g \le \left(\tfrac{1}{\sqrt{3}}+\varepsilon_t\right)\tfrac{1}{\sqrt{2}}\varepsilon_g \le \left(\tfrac{1}{\sqrt{3}}+\tfrac{1}{3}\right)\tan\tfrac{1}{3\sqrt{2}} \approx 0.11 \le \tfrac{1}{2}.$$

Now we bound the terms in the formula above: because $\varepsilon_t \le 1$, we have $2(1+\widetilde{t}_i^2) = O(1)$; and because $\frac{1}{\sqrt{2}}\varepsilon_g \le \frac{1}{3\sqrt{2}} \approx 0.24 < \pi/2$, we have $\frac{1}{\sqrt{2}}\varepsilon_g = O(\varepsilon_g)$. Plugging these bounds in, we obtain $\left|\tan\frac{\widetilde{\alpha}_i}{2}-\widetilde{t}_i\right| = O(\varepsilon_g)$, so $\left|\tan\frac{\widetilde{\alpha}_i}{2}-t_i\right| = O(\varepsilon_g+\varepsilon_t)$.

Finally we claim that $\prod_{i\in S}\widetilde{p}_i = \prod_{i\in S}p_i \pm O(n\varepsilon_g + n\varepsilon_t)$, where $\widetilde{p}_i = \frac{1-\tan\frac{\widetilde{\alpha}_i}{2}}{1+\tan\frac{\widetilde{\alpha}_i}{2}}$. Similar to the argument above, we show that $\widetilde{p}_i = p_i \pm O(\varepsilon_g+\varepsilon_t)$:

$$\begin{aligned}|\widetilde{p}_i - p_i| &= \left|\frac{1-\tan\frac{\widetilde{\alpha}_i}{2}}{1+\tan\frac{\widetilde{\alpha}_i}{2}}-\frac{1-\tan\frac{\alpha_i}{2}}{1+\tan\frac{\alpha_i}{2}}\right| \\ &= \left|\frac{1-t_i\pm O(\varepsilon_g+\varepsilon_t)}{1+t_i\pm O(\varepsilon_g+\varepsilon_t)}-\frac{1-t_i}{1+t_i}\right| \\ &= \left|\frac{\pm O(\varepsilon_g+\varepsilon_t)}{1+t_i\pm O(\varepsilon_g+\varepsilon_t)}\right| \\ &= O(\varepsilon_g+\varepsilon_t),\end{aligned}$$

by setting c larger than the constant c_1 in the denominator O notation so that $c_1(\varepsilon_g+\varepsilon_t) \le \frac{2}{3}$, so $1+t_i \pm c_1(\varepsilon_g+\varepsilon_t) \ge \frac{1}{3}$. Because $p_i \in (0.26, 1)$, we can convert this absolute error bound

into a relative error bound: $\widetilde{p}_i/p_i = 1 \pm O(\varepsilon_g + \varepsilon_t)$. Therefore

$$\prod_{i \in S} \widetilde{p}_i = \prod_{i \in S} p_i \pm O(n(\varepsilon_g + \varepsilon_t)). \tag{19}$$

This error bound gives us a lower bound on the precision ε in our output instance of finite-precision degree-4 flat-foldable rigid foldability. Namely, if $\varepsilon > \varepsilon_{\mathrm{LB}} := c_2 n(\varepsilon_g + \varepsilon_t)$, where c_2 is the constant in the O notation in Equation (19), then the finite-precision rigid foldability instance has a "yes" answer whenever $\prod \widetilde{p}_i = 1$, i.e., when the Partition instance has a "yes" answer.

It remains to prove that, if the Partition instance has a "no" answer, then the constructed crease pattern is a "no" instance to finite-precision rigid foldability. For this property to hold, we need an upper bound on ε. Consider a candidate partition $(S, A \setminus S)$, and suppose that $\Sigma(S) \neq \Sigma(A \setminus S)$. Because $A \subset \mathbb{N}$, $|\Sigma(S) - \Sigma(A \setminus S)| \geq 1$. Thus, for Inequality (9) to (incorrectly) hold on the constructed crease pattern, we would need ε to be at least

$$\begin{aligned}
\varepsilon'_{\mathrm{UB}} &= \left| \prod_i \widetilde{p}_i - 1 \right| \\
&= \left| \prod_i p_i - 1 \pm O(n(\varepsilon_g + \varepsilon_t)) \right| \\
&= \left| \frac{\exp(\Sigma(S)/\Sigma(A))}{\exp(\Sigma(A \setminus S)/\Sigma(A))} - 1 \pm O(n(\varepsilon_g + \varepsilon_t)) \right| \\
&= \left| \exp\left(\frac{\Sigma(S) - \Sigma(A \setminus S)}{\Sigma(A)} \right) - 1 \pm O(n(\varepsilon_g + \varepsilon_t)) \right| \\
&\geq \left| \exp\left(\frac{1}{\Sigma(A)} \right) - 1 \pm O(n(\varepsilon_g + \varepsilon_t)) \right| \\
&\geq \left| \frac{1}{\Sigma(A)} \pm O(n(\varepsilon_g + \varepsilon_t)) \right|,
\end{aligned}$$

where the last inequality is by the Taylor expansion of $\exp(1/\Sigma(A))$. Assuming $c \geq c_2$ where c_2 is the (same) constant in the O notation, we have $c_2 n(\varepsilon_g + \varepsilon_t) < \frac{1}{\Sigma(A)}$, so the absolute value operation is unnecessary, and we obtain

$$\varepsilon'_{\mathrm{UB}} \geq \frac{1}{\Sigma(A)} - cn(\varepsilon_g + \varepsilon_t) =: \varepsilon_{\mathrm{UB}}.$$

By setting $\varepsilon < \varepsilon_{\mathrm{UB}}$ (and thus $< \varepsilon'_{\mathrm{UB}}$), we guarantee that "no" answers are preserved.

To guarantee that $\varepsilon_{\mathrm{LB}} < \varepsilon_{\mathrm{UB}}$, we need that $c_2 n(\varepsilon_g + \varepsilon_t) < \frac{1}{\Sigma(A)} - c_2 n(\varepsilon_g + \varepsilon_t)$, i.e., $2c_2 n(\varepsilon_g + \varepsilon_t) < \frac{1}{\Sigma(A)}$, which holds if $c \geq c_2$. Thus it suffices to set c to the integer $\lceil \max\{c_1, c_2\} \rceil$, enabling us to compute and represent $\varepsilon_g = \varepsilon_t = \frac{1}{3cn\Sigma(A)}$ exactly as a rational number.

Therefore, by setting $\varepsilon = \frac{\varepsilon_{\mathrm{LB}} + \varepsilon_{\mathrm{UB}}}{2}$ (also computable exactly as a rational number), we obtain $\varepsilon_{\mathrm{LB}} < \varepsilon < \varepsilon_{\mathrm{UB}}$ as needed for correctness of the reduction. All (rational) coordinates in the reduction have numerator and denominator bounded by a constant-degree polynomial in $1/\varepsilon_g = 3cn\Sigma(A)$, and thus so does the output number ε. □

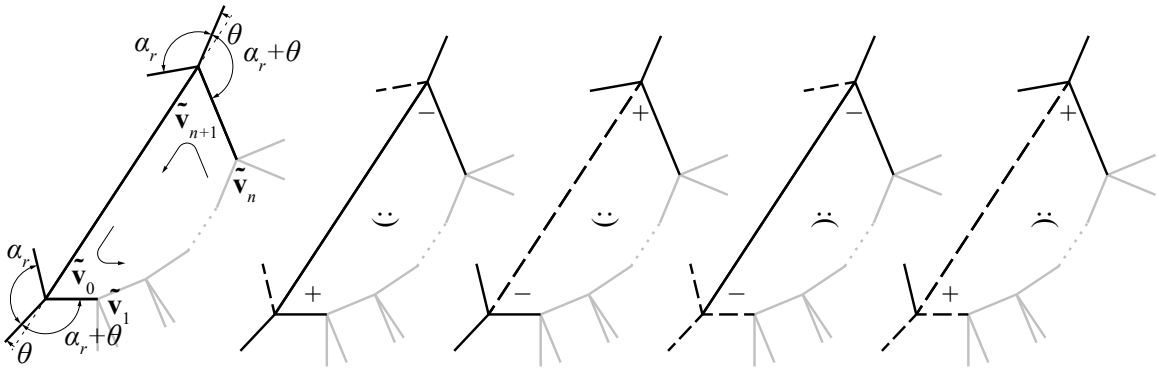

Figure 8: Fixing the crease pattern to avoid collinear creases.

Corollary 3.2. *Finite-precision degree-4 flat-foldable rigid foldability with optional creases is weakly* NP*-complete.*

Proof. Again Theorem 2.12 establishes membership in NP. To prove weak NP-hardness, we use a slight variation of the reduction in Theorem 3.1. Most vertices in the reduction have the property that, if any incident crease strictly folds, then all four incident creases must fold. The two exceptions are $\widetilde{\mathbf{v}}_0$ and $\widetilde{\mathbf{v}}_{n+1}$, each having two creases such that all four of these creases lie on a line. So the construction as is always has a rigid folding motion with optional creases: fold along that line.

To fix this, we simply rotate the incident terminal creases in a consistent way; refer Figure 8. Specifically, we rotate $\widetilde{\mathbf{v}}_0\widetilde{\mathbf{c}}_0$ and $\widetilde{\mathbf{v}}_0\widetilde{\mathbf{b}}_0$ clockwise by angle $\theta \in (0, \pi - \alpha_r)$, and we rotate $\widetilde{\mathbf{v}}_{n+1}\widetilde{\mathbf{c}}_{n+1}$ and $\widetilde{\mathbf{v}}_{n+1}\widetilde{\mathbf{b}}_{n+1}$ counterclockwise by the same angle θ. To ensure that this rotation can be done exactly with rational coordinates, we set the tangent of half angle to be rational and apply the rotation matrix of Equation (18), e.g., $\theta = 2\arctan\frac{1}{6} \approx 18.9°$. Because vertices $\widetilde{\mathbf{v}}_{n+1}$ and $\widetilde{\mathbf{v}}_0$ are mirror symmetric, if the speed coefficient at vertex $\widetilde{\mathbf{v}}_{n+1}$ is denoted by $p_{r,+}$ (call this mode +) or $p_{r,-}^{-1}$ (call this mode −), then the speed coefficient at vertex $\widetilde{\mathbf{v}}_0$ is $p_{r,-}$ (call this mode +) or $p_{r,+}^{-1}$ (call this mode −). We can compute $p_{r,+}$ and $p_{r,-}$ by combining Equations (3)–(5) with α, β set to $\alpha_r + \theta, \alpha_r$ (see Figure 2, replacing L_0 with $\widetilde{\mathbf{v}}_n\widetilde{\mathbf{v}}_{n+1}$ and L_3 with $\widetilde{\mathbf{v}}_{n+1}\widetilde{\mathbf{v}}_0$):

$$p_{r,+} = p_+(3,0) = p_+(\alpha_r + \theta, \alpha_r) = \frac{1 - \tan\frac{\alpha_r}{2}\tan\frac{\alpha_r+\theta}{2}}{1 + \tan\frac{\alpha_r}{2}\tan\frac{\alpha_r+\theta}{2}}; \tag{20}$$

$$p_{r,-} = p_-(3,0) = -p_-(\alpha_r + \theta, \alpha_r) = \frac{\tan\frac{\alpha_r+\theta}{2} - \tan\frac{\alpha_r}{2}}{\tan\frac{\alpha_r+\theta}{2} + \tan\frac{\alpha_r}{2}}. \tag{21}$$

We claim that the modes at $\widetilde{\mathbf{v}}_{n+1}$ and $\widetilde{\mathbf{v}}_0$ need to be either $(+,-)$ or $(-,+)$ in order to be rigidly foldable (Figure 8, middle two images). Assuming this claim, Equation (13) applies and the rest of the proof follows. To prove the claim, we use that $p_{r,+} < 0$ and $p_{r,-} > 0$ for $\theta \in (0, \pi - \alpha_r)$ and $\alpha_r \in (150°, 157.5°)$ because $\tan\frac{\alpha_r+\theta}{2} > \tan\frac{\alpha_r}{2} > 1$. Thus, mode assignment $(+,+)$ or $(-,-)$ would induce a negative speed coefficient $p_{r,+}p_{r,-}$ or $p_{r,+}^{-1}p_{r,-}^{-1}$, respectively, from crease $\widetilde{\mathbf{v}}_n\widetilde{\mathbf{v}}_{n+1}$ to crease $\widetilde{\mathbf{v}}_0\widetilde{\mathbf{v}}_1$, i.e., the mountain–valley assignment switches between

the creases (Figure 8, right two images). This contradicts that the creases $\widetilde{\mathbf{v}}_i\widetilde{\mathbf{v}}_{i+1}$ for $0 \leq i \leq n$ all have the same mountain–valley assignment. Therefore mode assignments $(+,+)$ and $(-,-)$ are impossible, leaving only the desired assignments $(+,-)$ and $(-,+)$, so the proof proceeds as before. □

4 Rigid Foldability with Optional Creases is Strongly NP-hard

Theorem 4.1. *Rigid foldability with optional creases is strongly* NP*-hard.*

To prove this theorem, we reduce from *Positive 1-in-E3 SAT*: given a set of m *clauses*, each consisting of exactly three variables (without negation), decide whether the variables can be set to true or false such that every clause has exactly one true variable (and exactly two false variables). This problem is known to be NP-hard [23, 24]. Figure 9 shows the crease pattern for such a Positive 1-in-E3 SAT reduction, i.e., the crease pattern is rigidly foldable if and only if there is a set of binary variables that satisfy a given Positive 1-in-E3 SAT problem. The basic idea is that we describe binary variables by whether creases are folded (true) or not (false). This binary information will be carried via sets of four parallel creases, which we call *wires*. We then design *gadgets*, which are crease patterns connected to wires that are designed to be rigidly foldable for certain desired binary patterns of wires.

Figure 10 shows a schematic diagram for the overall design of the crease pattern in Figure 9, using iconography to represent different types of wires and gadgets. Each gadget consists of a local crease pattern with rational vertex coordinates within a constant-size rectangle, whose top and bottom sides connect to one vertical wire and whose left and right sides connect to one or more horizontal wires. Specifically, we design a *splitter gadget* (Figure 12) that copies a horizontal value to a vertical value and vice versa; a *crossover gadget* (Figure 14 right) that enables a horizontal and vertical value to cross without influencing each other; a *suppressor gadget* (Figure 14 left) that more simply crosses a horizontal and a vertical while requiring a NAND constraint (not both are true);[1] and a *clause gadget* (Figure 16) that rigidly folds if and only if exactly one of three horizontal inputs are true. The gadgets are arranged in the crease pattern as follows (see Section 4.2 for more detail):

1. The bottom n horizontal wires represent the input variables $x_1, x_2, \ldots, x_n$. Each variable can be brought to each clause that uses it using two split gadgets, one to bend the variable horizontal wire to a vertical wire, and the second to bring the vertical wire to a horizontal wire of the clause.

2. Each set of four horizontal wires above the input variables section correspond to a clause. The copied variables in the vertical lines are reflected horizontally using a 3×3 grid of gadgets composed of splitters and suppressors. These gadgets force at most one of the three variables to be true, and the folding of the clause gadget itself will ensure that exactly one of the horizontal wires must be true.

[1] The conceptual complexity of the reduction could be reduced by replacing every suppressor gadget with a crossover gadget, at the cost of increasing the combinatorial complexity of the figures by a constant factor.

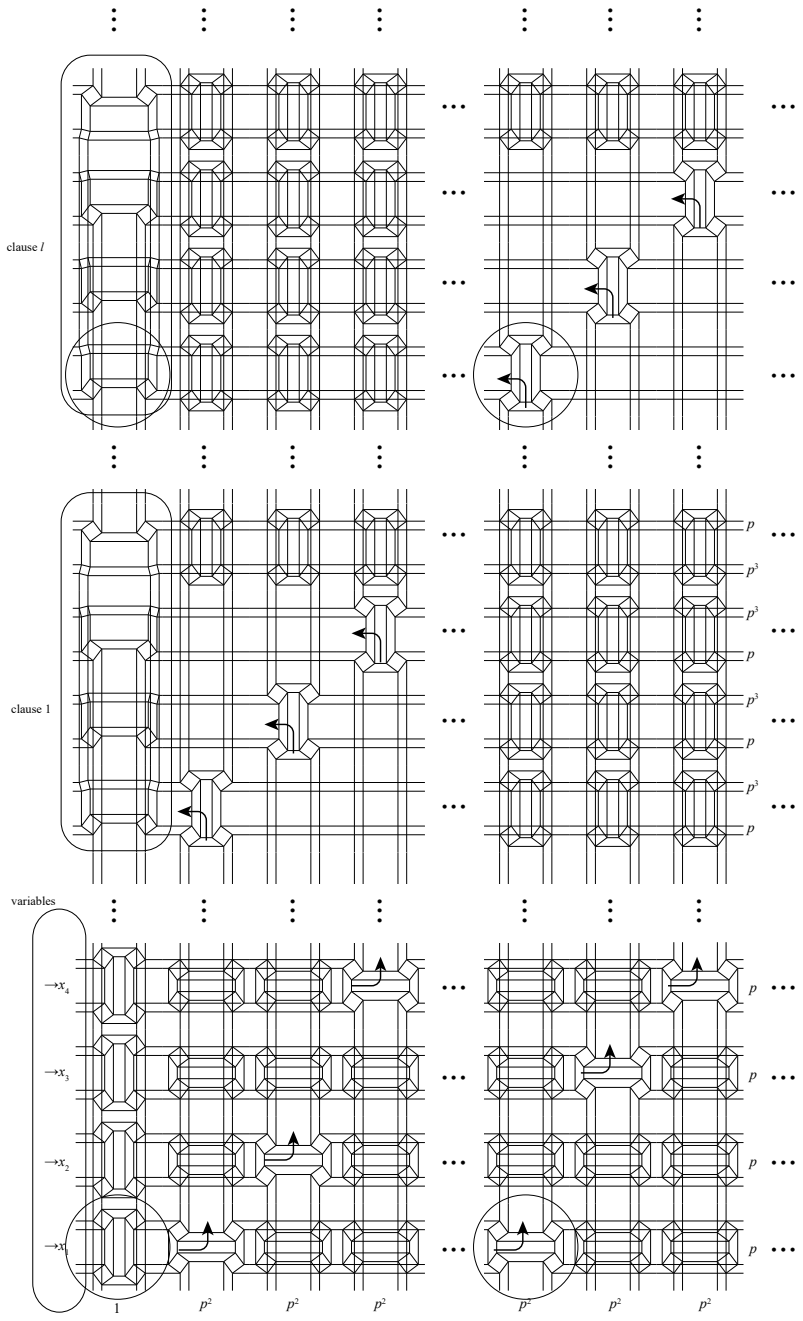

Figure 9: A crease pattern rigidly foldable if and only if a Positive 1-in-E3 SAT formula is satisfiable.

To prove that this reduction works, we use the following strategy. For each gadget, (1) we show that it successfully constrains the binary operations, i.e., it keeps wrong patterns from folding (the "only if" part), and (2) we give one mountain–valley assignment and rigid folding mode for each possible case of true and false (the "if" part). The first part ensures

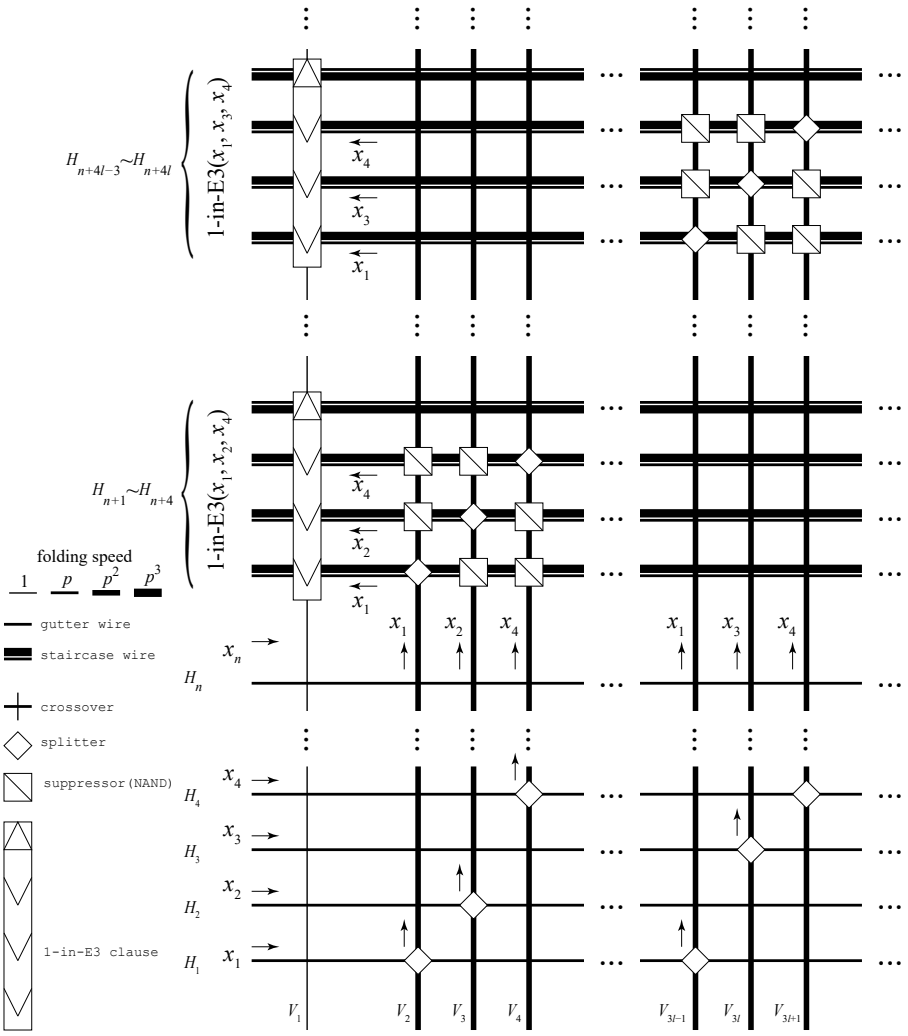

Figure 10: Schematic diagram of gadget layout. Line thickness represents folding speed, ranging from 1 (thinnest) to p^3 (thickest).

that rigid folding of the pattern guarantees that Positive 1-in-E3 SAT can be solved, while the second part shows that any solution to Positive 1-in-E3 SAT guarantees at least one assignment that makes the pattern rigidly foldable.

4.1 Gadgets

4.1.1 Wires

A *wire* is represented by four parallel lines with small, large, small spacing as in Figure 11. We call an optional-crease folding of this local crease pattern *true* if any of the four creases fold, and *false* if none of the four creases fold.

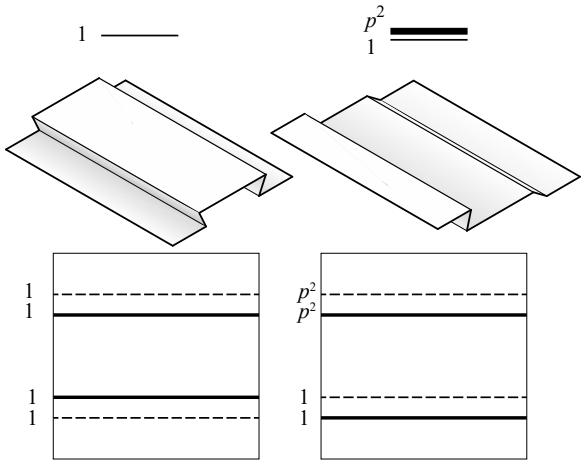

Figure 11: Two types of wire gadgets in true setting. Left: gutter wire. Right: staircase wire. The numbers indicate relative folding speed.

For true values, we use two rigid folding modes of wires, called *gutter* and *staircase* respectively; see Figure 11. Note that the folding speeds measured in tangents of half the fold angles are different between two pairs of creases for a staircase wire. In our construction, we will use a folding speed of $p = \frac{1}{2}$, and the relative speed of the pairs of creases in a staircase will be $p^2 = \frac{1}{4}$.

4.1.2 Splitters

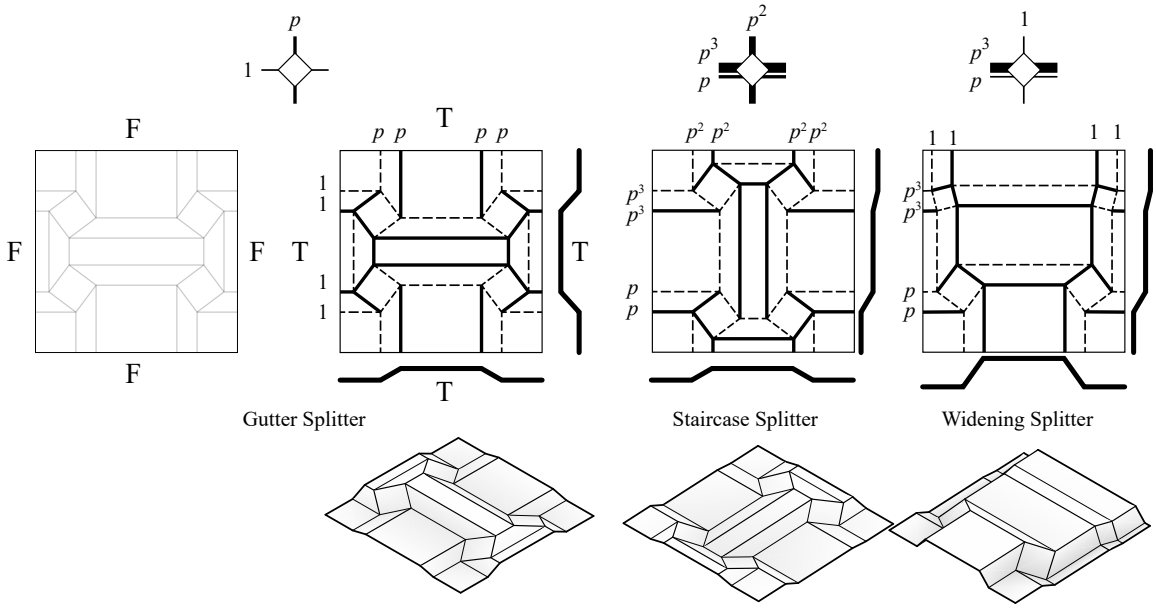

Figure 12: Splitter gadget allowing for (true, true) or (false, false) only.

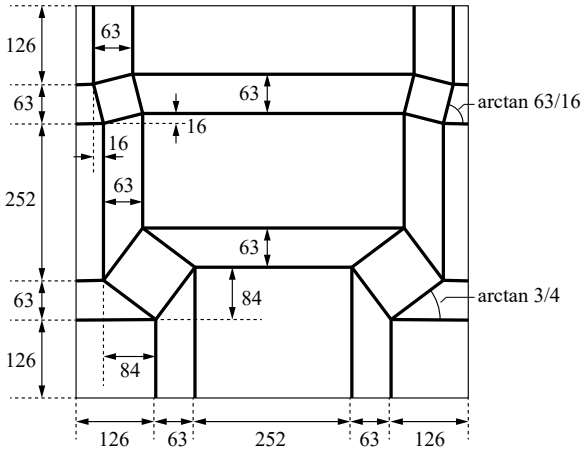

Figure 13: Dimensions of widening splitter given as integers. All other gadgets are placed along the same integer grid.

We define three types of splitter gadgets for connecting different types of wires; refer to Figure 12. A *gutter splitter* is a 2×2 twist-fold tessellation consisting of four square twist folds with a minimum sector angle of $\arctan \frac{3}{4}$, where the left and right horizontal wires are the input and the top and bottom vertical wires are the output (or the other way around). Note that we may think of both the left and right wires as inputs (and both top and bottom wires as outputs) because wire signals will always be unchanged as they travel through the splitter, either horizontally or vertically. A standard splitter will have all of its wires be gutters. A *staircase splitter* is a 90° rotation of the gutter splitter, but its wires will have different modes so that the horizontal wire is a staircase and the vertical wire is a gutter. A *widening splitter* uses a pattern with two pairs of twists with minimum sector angles $\arctan \frac{3}{4}$ (at the bottom) and $2 \arctan \frac{7}{9} = \arctan \frac{63}{16}$ (at the top) to change the widths of vertical wires. The folding mode of a widening splitter is designed to match with staircase horizontal wires and gutter vertical wires.

These gadgets all have integer coordinates. Figure 13 gives the dimensions for a widening splitter. The gutter splitter's crease pattern is a reflection of the bottom half of the widening splitter to replace the top half, so it also has integer coordinates. The staircase splitter's crease pattern is a 90° rotation of the gutter splitter, so it too has integer coordinates.

We denote the binary values of a gadgets' incident wires with the notation (X, Y) where X is the boolean value of the horizontal wires and Y is the value of the vertical wires.

Lemma 4.2. *A gutter splitter, staircase splitter, and widening splitter can fold only if they copy the values in the input to the output, and thus the possible patterns are (true, true) and (false, false).*

Proof. All horizontal creases are connected to vertical creases via degree-4 vertices with finite speed coefficients. If any of these creases fold, then every fold line in the gadget must fold, forcing the input and the output wires to have the same value. □

Lemma 4.3. *A gutter splitter, staircase splitter, and widening splitter can rigidly fold in the mode specified in Figure 12, where the numbers* $1, p, p^2, p^3$ *(*$p = \frac{1}{2}$*) assigned to the fold lines are the absolute relative folding speeds measured in tangent of half the fold angles.*

Proof. All splitters are composed of four rigid origami twists, as in Section 2.5. By consecutively mirroring the square twist in mode (a) of Figure 3 across horizontal and vertical axes, we obtain a gutter splitter with the folding mode described in Figure 12 (left two). Because $p(\arctan \frac{3}{4}) = \frac{1}{2}$, the folding follows the specified speeds.

The staircase splitter is obtained by rotating the normal splitter, but then changing some of the modes of the vertices (refer to Figure 2) so as to cascade the relative folding speed p as shown in Figure 12. A widening splitter connects mode (a) of the square twist from Figure 3 with another square twist with a different minimum sector angle. The consistent folding mode is ensured by having the bottom and top twists connected through folds with the same absolute speed and then having them mirrored with respect to the vertical line. Now, because we chose $p(\arctan \frac{63}{16}) = \frac{1}{8}$ for the top twists, the top two creases fold at p^2 times the speed of the bottom two creases. □

Remark 4.4. All vertical wires are gutters. In the gutter splitter, the speed of the vertical wire is p times the speed of the horizontal wire. In the staircase splitter, the speed of the vertical wire is p^2 times that of the widening splitter (when we synchronize the horizontal staircase wires of staircase and widening splitters).

4.1.3 Suppressor and Crossover Gadgets

Just overlaying two orthogonal wires (Figure 14 left, which has integer coordinates) makes the vertical and horizontal wires suppress each other so that they cannot be rigidly folded at the same time (a NAND constraint). We call this gadget a *suppressor*, which allows only the patterns (false, false), (true, false), and (false, true).

Lemma 4.5. *A suppressor leaves all four horizontal creases unfolded or all four vertical creases unfolded.*

Proof. Every horizontal crease crosses every vertical crease perpendicularly, forming a degree-4 vertex with 90° sector angles. Because the speed coefficients are 0 at such a point, no vertical crease can fold if any horizontal crease has fold angle in $(0, 180°)$, and vice versa. □

We also need a crossover system to avoid logical interactions between unrelated horizontal and vertical wires.

A *crossover gadget* (Figure 14, right) is realized by overlaying the crease pattern of a splitter on top of a suppressor, where we line up the horizontal and vertical inputs. Thus there are three different crossover gadgets, just like splitter gadgets (Figure 15). Because each individual pattern has integer coordinates, their overlay has rational vertex coordinates. The overlaying of patterns allows us to choose either pattern to be active, so we get the union of the folding modes of splitters and suppressor, which complete four possible binary patterns.

Lemma 4.6. *Crossover gadgets can fold into the four patterns (false, false), (true, false), (false, true) and (true, true). The folding modes of the (true, false) and (false, true) patterns follow those of the corresponding wires, and the folding mode of the (true, true) pattern follows that of a splitter.*

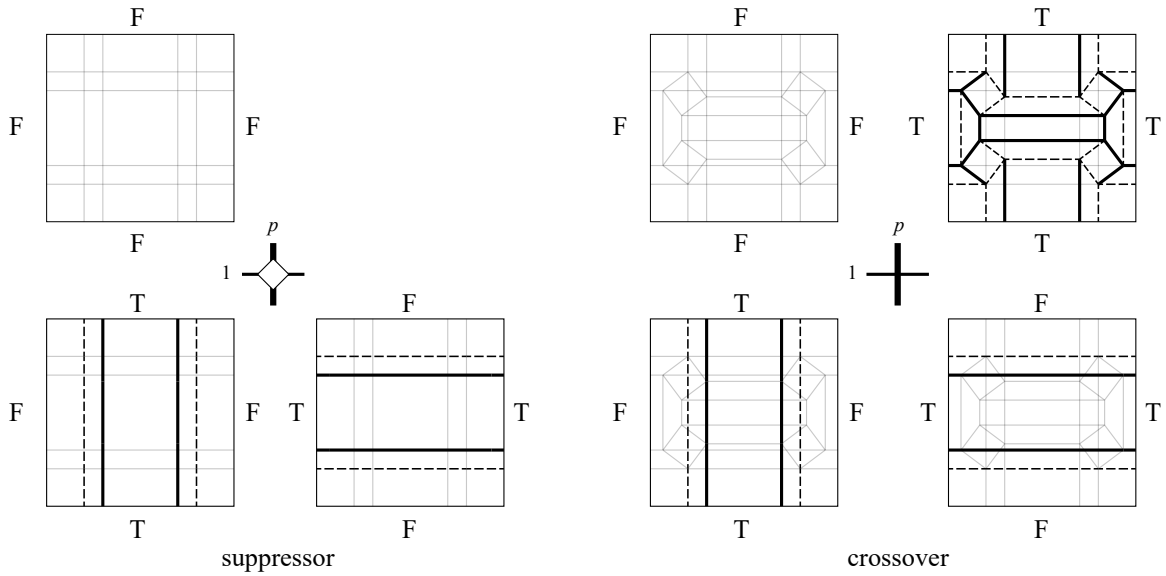

Figure 14: Suppressor (left) cannot achieve (true, true) pattern. Crossover gadget (right) can realize any combination (false, false) (false, true), (true, false), (true, true).

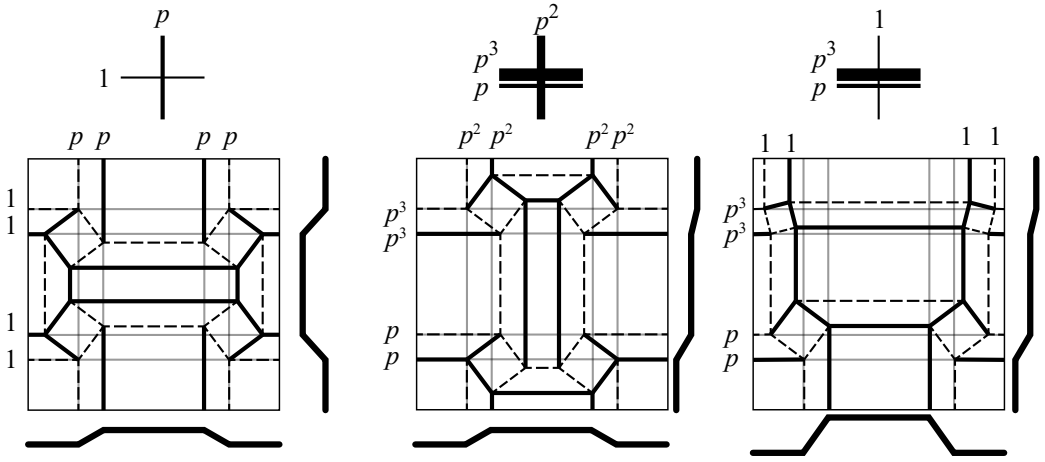

Figure 15: Three types of crossover gadgets corresponding to different combinations of wires and folding speed.

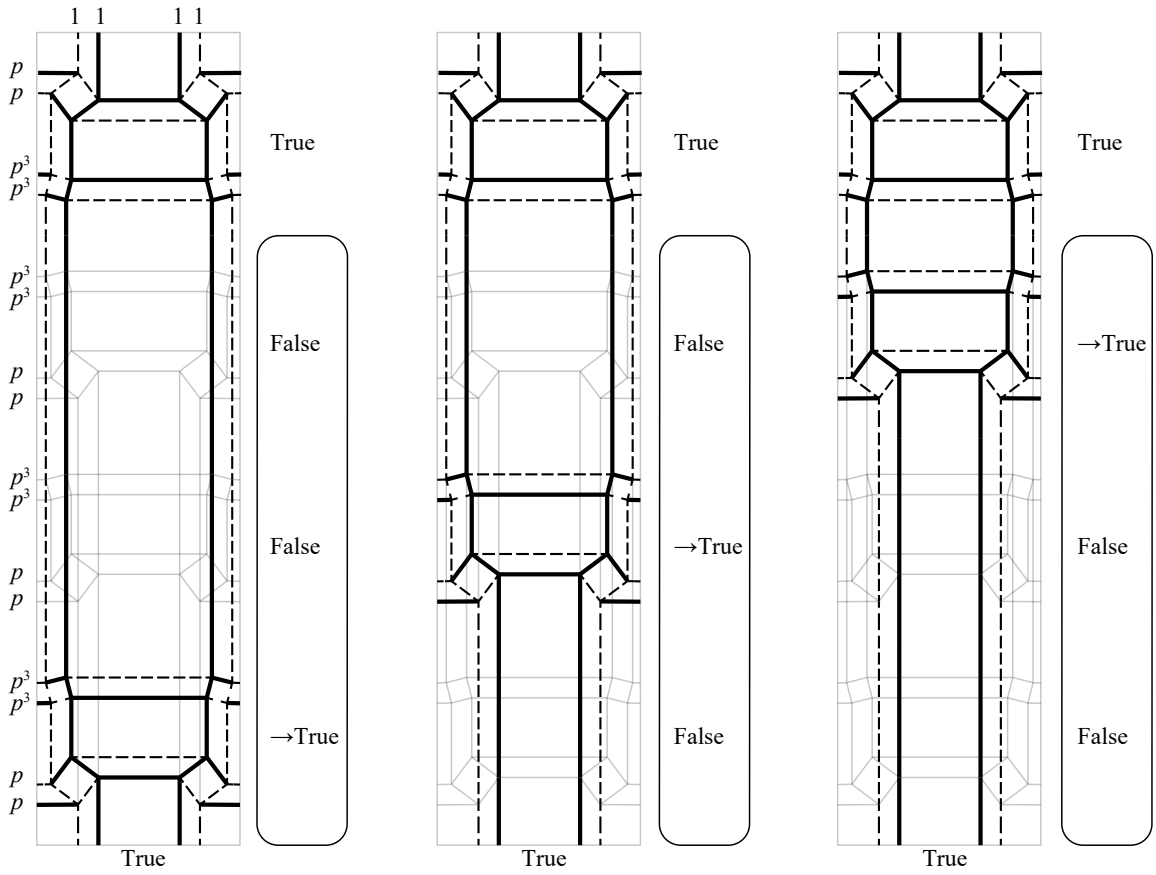

Figure 16: Clause gadget. If the vertical wire is true, then this gadget can fold in three ways. Each folding mode corresponds to horizontal wires (true, false, false), (false, true, false), or (false, false, true), forcing exactly one of the horizontal wires to be true.

4.1.4 Clause Gadget

A *clause gadget* is designed by overlaying three widening splitters in vertical direction, connected by one upside-down widening splitter on top (see Figure 16). Because each individual pattern has integer coordinates, their overlay has rational vertex coordinates. We consider the three bottom horizontal wires to be the literals, and the vertical wire gives the satisfiability. The fourth (top) horizontal wire, which is connected to the upside-down widening splitter, exists only for readjustment of widths to connect to the next clause on top.

Lemma 4.7. *A clause gadget folds only if exactly one of three inputs is true.*

Proof. Assume that the second input wire (from the bottom) is true. Because every horizontal crease in a clause gadget stops when it encounters a twist fold, all the twists must be folded in the second wire section. The vertical wires above the twists are wide, and the vertical wires below the twists are narrow. Therefore the twists connected to the first and

third input wires will be suppressed, and the clause must form a (false, true, false) pattern. The same argument works for the first and third horizontal wires, so we obtain (true, false, false) or (false, false, true) patterns. Because the bottommost vertical wire is narrow and the topmost vertical wire is wide, the vertical wire is foldable only if it uses at least one of the twists, but doing so will force us to choose one of three modes we have described. □

Lemma 4.8. *Clause gadget can fold in the three modes specified in Figure 16, which follows the folding mode of a widening splitter and its upside-down mirror image.*

Proof. The rigid folding motion follows that of widening splitter, and because the connected upside-down splitter is compatible, they fold rigidly with the specified relative speed (in tangent-half-fold-angle parameterization) in Figure 16. □

4.2 Proof and Layout

Proof of Theorem 4.1. Given a Positive 1-in-E3 SAT formula $R_1 \wedge R_2 \wedge \cdots \wedge R_m$ with m clauses $R_1, R_2, \ldots, R_m$ of n variables $x_1, x_2, \ldots, x_n$, we construct a grid of $n+4m$ horizontal wires $H_1, H_2, \ldots, H_{n+4m}$ and vertical wires $V_1, V_2, \ldots, V_{3m+1}$, where we place a gadget at each intersection node of wires or at groups of nodes as specified below. By default, crossover gadgets are placed at unspecified nodes between horizontal and vertical wires.

We set the horizontal wires from $H_1, H_2, \ldots, H_n$ to be the variables $x_1, \ldots, x_n$, and each set of four horizontal wires $(H_{n+4(l-1)+1}, \ldots, H_{n+4(l-1)+4})$ to be the lth clause R_l $(l = 1, 2, \ldots, m)$. Specifically, for $R_l = (x_i, x_j, x_k)$, we place a clause gadget at the intersection between V_1 and $(H_{n+4(l-1)+1}, \ldots, H_{n+4(l-1)+4})$. The input variables $H_{n+4(l-1)+1}$, $H_{n+4(l-1)+2}, H_{n+4(l-1)+3}$ of the clause are copied from $V_{3l-1}, V_{3l}, V_{3l+1}$, respectively; and the values of $V_{3l-1}, V_{3l}, V_{3l+1}$ are copied from H_i, H_j, H_k, respectively, by placing splitters at the appropriate intersections. We claim that the value of each of the vertical wires $V_{3l-1}, V_{3l}, V_{3l+1}$ is constrained only by the clause gadgets that they are attached to via splitters. This is because each of these vertical wires, if folding in a true wire, will (1) suppress the other vertical wires being fed into this clause and (2) cross other horizontal wires at a crossover gadget which will not change its value. By Lemmas 4.2, 4.5, 4.6 and 4.7, each clause can rigidly fold only if the clause returns true.

Now, because we concatenate all cause gadgets along V_1, all clauses must be true if any clause is true. We claim that at least one clause must be true if any fold line is folded, therefore the whole laid out pattern can fold only if the given Positive 1-in-E3 SAT formula $R_1 \wedge R_2 \wedge \cdots \wedge R_m$ is satisfied. The claim follows because, if all the clauses are false, then all variables are false and thus all horizontal wires are false. Because all vertical wires $V_2, \ldots, V_{3m+1}$ are the copies of variables, all vertical wires are also false, and thus the material remains completely unfolded.

If the Positive 1-in-E3 SAT formula is satisfiable, we may assign true and false to each wire as appropriate. For false wires, we can assume that they are removed from the crease pattern, which will result in a degree-4 flat-foldable mesh composed of gutter splitters, staircase splitters, widening splitters. For these creases, we assign the specified folding modes in Lemmas 4.3 and 4.8, so that they are compatible through the gutter and

staircase wires at correct speeds. In particular, the synchronization between the widening and staircase splitters is realized by the different speeds between V_1 (with speed 1) and $V_2, \ldots, V_{3m+1}$ (with speed p^2) as in Remark 4.4. To allow for correct synchronization, we place 90°-rotated crossovers at the intersections between V_1 and $H_1, H_2, \ldots, H_n$ so that the speed of the horizontal wire is p times the speed of the vertical wire; see the circled parts of Figure 9 and the zoomed-in subpattern of Figure 17. More precisely, if the lth clause's dth variable (where $d \in \{0, 1, 2\}$) is x_i which is true, then each cycle formed by (1) the gutter splitter at (V_{3l-1+d}, H_i), (2) the staircase splitter at $(V_{3l-1+x}, H_{n+4l-3+d})$, (3) the widening splitter at $(V_1, H_{n+4l-3+x})$ as a part of clause gadget, and (4) the 90°-rotated splitter at (V_1, H_i) as a part of crossover gadget rigidly folds with synchronized speeds at the creases.

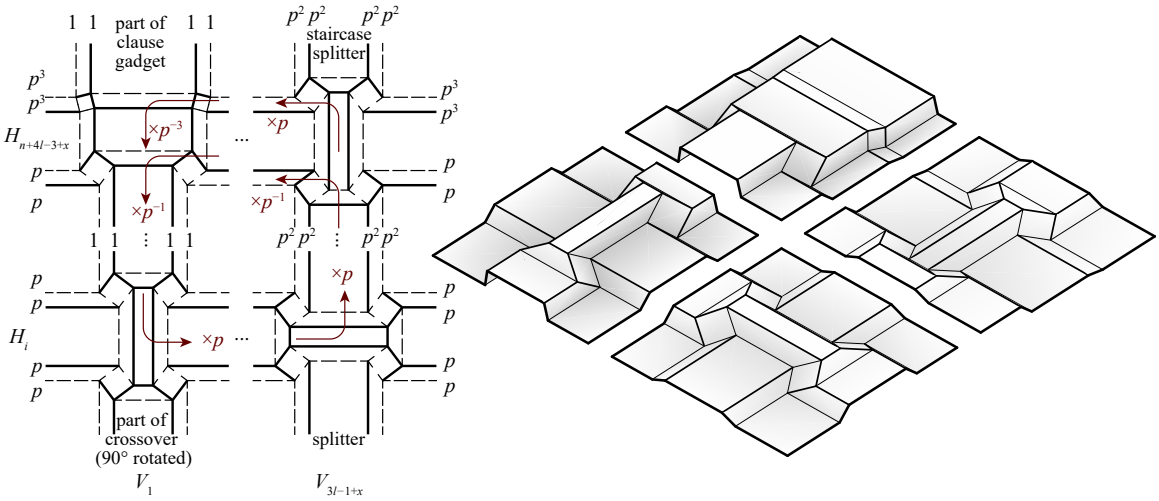

Figure 17: Synchronization of the gadgets: gutter splitter (right bottom), staircase splitter (right top), widening splitter from a clause gadget (left top), and 90°-rotated splitter from a 90°-rotated crossover (left bottom). An example set of these four gadgets is marked with circles in Figure 9.

Because all gadgets have rational coordinates, so does the constructed crease pattern. □

5 Conclusion

We have shown weak NP-completeness of rigid foldability up to finite precision of a degree-4 flat-foldable crease pattern, using all or optional creases (Theorem 3.1); and strong NP-hardness of exact rigid foldability with optional creases (Theorem 4.1); refer to Table 1.

On the hardness side, two natural questions are whether any all-crease rigid foldability problem is strongly NP-hard; and whether exact rigid foldability using all creases is NP-hard (weakly or strongly). Weak NP-hardness seems to bump into precision issues, so it might be easiest to solve both problems simultaneously by proving strong NP-hardness of exact rigid foldability using all creases.

On the algorithmic side, the main open question is whether rigid foldability of general crease patterns is in NP, beyond the degree-4 flat-foldable case that we showed is in NP (Theorem 2.12). As rigid origami is a special case of linkage folding, the rigid foldability problem belongs to the class $\exists\mathbb{R}$ [2]. Is deciding rigid foldability of a flat crease pattern $\exists\mathbb{R}$-hard like linkage folding [2]?

Another interesting direction would be to generalize our notion of finite-precision rigid foldability beyond just degree-4 flat-foldable crease patterns (as in Definition 2.11). Some initial steps in this direction are made in [10]. With such a definition in hand, we could ask whether (non-degree-4) finite-precision rigid foldability is in NP.

Acknowledgements

Tomohiro Tachi supported by KAKENHI 16H06106. Thomas Hull supported by NSF EFRI-1240441 and DMS-1906202. Hugo A. Akitaya supported by NSF CCF-1422311 and CCF-1423615. This work was begun at the 2015 Bellairs Workshop on Computational Geometry, co-organized by Erik Demaine and Godfried Toussaint. We thank the other participants of the workshop for stimulating discussions.

References

[1] Zachary Abel, Jason Cantarella, Erik D. Demaine, David Eppstein, Thomas C. Hull, Jason S. Ku, Robert J. Lang, and Tomohiro Tachi. Rigid origami vertices: conditions and forcing sets. *Journal of Computational Geometry*, 7(1):171–184, 2016.

[2] Zachary Abel, Erik D. Demaine, Martin L. Demaine, Sarah Eisenstat, Jayson Lynch, and Tao B. Schardl. Who needs crossings? hardness of plane graph rigidity. In *Proceedings of the 32nd International Symposium on Computational Geometry*, pages 3:1–3:15, Boston, MA, June 2016.

[3] Hugo A. Akitaya, Kenneth C. Cheung, Erik D. Demaine, Takashi Horiyama, Thomas C. Hull, Jason S. Ku, Tomohiro Tachi, and Ryuhei Uehara. Box pleating is hard. In *Revised Papers from the 18th Japan Conference on Discrete and Computational Geometry and Graphs*, pages 167–179, Kyoto, Japan, September 2015.

[4] sarah-marie belcastro and Thomas C. Hull. Modelling the folding of paper into three dimensions using affine transformations. *Linear Algebra and its Applications*, 348:273–282, 2002.

[5] Marshall Bern and Barry Hayes. The complexity of flat origami. In *Proceedings of the 7th ACM-SIAM Symposium on Discrete Algorithms (SODA '96)*, pages 175–183, 1996.

[6] J. M. Borwein and P. B. Borwein. On the complexity of familiar functions and numbers. *SIAM Review*, 30(4):589–601, 1988.

[7] Raoul Bricard. Mémoire sur la théorie de l'octaèdre articulé. *Journal de Mathématiques Pures et Appliquées, 5e série*, 3:113–150, 1897.

[8] Christoph Burnikel, Stefan Funke, Kurt Mehlhorn, Stefan Schirra, and Susanne Schmitt. A separation bound for real algebraic expressions. *Algorithmica*, 55(1):14–28, September 2009.

[9] Jian S. Dai. Configuration transformation and mathematical description of manipulation of origami cartons. In K. Miura, T. Kawasaki, T. Tachi, R. Uehara, R. J. Lang, and P. Wang-Iverson, editors, *Origami^6: Proceedings of the 6th International Meeting of Origami Science, Mathematics, and Education*, pages 163–173. The American Mathematical Society, 2015.

[10] Erik D. Demaine, Martin L. Demaine, David A. Huffman, Thomas C. Hull, Duks Koschitz, and Tomohiro Tachi. Zero-area reciprocal diagram of origami. In K. Kawaguchi, M. Ohsaki, and T. Takeuchi, editors, *Proceedings of the IASS Annual Symposium 2016*, Tokyo, Japan, September 2016.

[11] Erik D. Demaine and Joseph O'Rourke. *Geometric Folding Algorithms: Linkages, Origami, Polyhedra*. Cambridge University Press, Cambridge, 2007.

[12] Thomas A. Evans, Robert J. Lang, Spencer P. Magleby, and Larry L. Howell. Rigidly foldable origami twists. In K. Miura, T. Kawasaki, T. Tachi, R. Uehara, R. J. Lang, and P. Wang-Iverson, editors, *Origami^6: Proceedings of the 6th International Meeting of Origami Science, Mathematics, and Education*, pages 119–130. The American Mathematical Society, 2015.

[13] Shuzo Fujimoto and Masami Nishikawa. 創造する折り紙遊びへの招待 / *Sōzō suru origami asobi e no shōtai (Invitation to Creative Playing with Origami, in Japanese)*. Asahi Culture Center, Tokyo, 1982.

[14] Michael R. Garey and David S. Johnson. *Computers and Intractability: A Guide to the Theory of NP-Completeness*. W. H. Freeman & Co., 1979.

[15] David Harvey and Joris van der Hoeven. Integer multiplication in time $O(n \log n)$. HAL Preprint hal-02070778, 2019. https://hal.archives-ouvertes.fr/hal-02070778.

[16] E. Hawkes, B. An, N. M. Benbernou, H. Tanaka, S. Kim, E. D. Demaine, D. Rus, and R. J. Wood. Programmable matter by folding. *Proceedings of the National Academy of Sciences of the United States of America*, 107(28):12441–12445, 2010.

[17] David A. Huffman. Curvature and creases: A primer on paper. *IEEE Transactions on Computers*, 25(10):1010–1019, 1976.

[18] Thomas Hull. *Project Origami: Activities for Exploring Mathematics*. A K Peters/CRC Press, Wellesley, MA, 2nd edition, 2012.

[19] Thomas C. Hull. Counting mountain-valley assignments for flat folds. *Ars Combinatoria*, 67:175–187, 2003.

[20] Thomas C. Hull. Rigid folding of periodic triangulated origami tessellations. In K. Miura, T. Kawasaki, T. Tachi, R. Uehara, R. J. Lang, and P. Wang-Iverson, editors,

Origami^6*: Proceedings of the 6th International Meeting of Origami Science, Mathematics, and Education*, pages 97–108. The American Mathematical Society, 2014.

[21] Richard M. Karp. Reducibility among combinatorial problems. In Raymond E. Miller, James W. Thatcher, and Jean D. Bohlinger, editors, *Proceedings of a Symposium on the Complexity of Computer Computations*, pages 85–103, March 1972.

[22] Toshikazu Kawasaki. On the relation between mountain-creases and valley-creases of a flat origami. In H. Huzita, editor, *Proceedings of the 1st International Meeting of Origami Science and Technology*, pages 229–237, Ferrara, Italy, December 1989. An unabridged Japanese version appeared in *Sasebo College of Technology Report*, 27:153–157, 1990.

[23] Philippe Laroche. Planar 1-in-3 satisfiability is NP-complete. *Comptes Rendus de l'Académie des Sciences, Serie I (Mathematiques)*, 316(4):389–392, 1993.

[24] Wolfgang Mulzer and Günter Rote. Minimum-weight triangulation is NP-hard. *Journal of the ACM*, 55(2):11:1–11:29, May 2008.

[25] S. A. Robertson. Isometric folding of Riemannian manifolds. *Proceedings of the Royal Society of Edinburgh*, 79(3–4):275–284, 1977.

[26] M. Schenk, S. G. Kerr, A. M. Smyth, and S. D. Guest. Inflatable cylinders for deployable space structures. In F. Escrig and J. Sánchez, editors, *Proc. of the First Conference Transformables 2013, In the Honor of Emilio Pérez Piñero, Seville, Spain*, Madrid, Spain, 2013. Starbook Editorial.

[27] Jesse L. Silverberg, Arthur A. Evans, Lauren McLeod, Ryan C. Hayward, Thomas Hull, Christian D. Santangelo, and Itai Cohen. Using origami design principles to fold reprogrammable mechanical metamaterials. *Science*, 345(6197):647–650, 2014.

[28] Tomohiro Tachi. Freeform rigid-foldable structure using bidirectionally flat-foldable planar quadrilateral mesh. In Cristiano Ceccato, Lars Hesselgren, Mark Pauly, Helmut Pottmann, and Johannes Wallner, editors, *Advances in Architectural Geometry 2010*, pages 87–102. Springer Vienna, 2010.

[29] Tomohiro Tachi. Rigid-foldable thick origami. In P. Wang-Iverson, R. J. Lang, and M. Yim, editors, *Origami*^{5}*: Proceedings of the 5th International Meeting of Origami Science, Mathematics, and Education*, pages 253–263, Boca Raton, FL, 2011. CRC Press.

[30] Tomohiro Tachi and Thomas C. Hull. Self-foldability of rigid origami. *Journal of Mechanisms and Robotics*, 9(2):021008–021017, 2016.